iScience

CellPress
OPEN ACCESS

Article

Mycolic acid-containing bacteria trigger distinct types of membrane vesicles through different routes

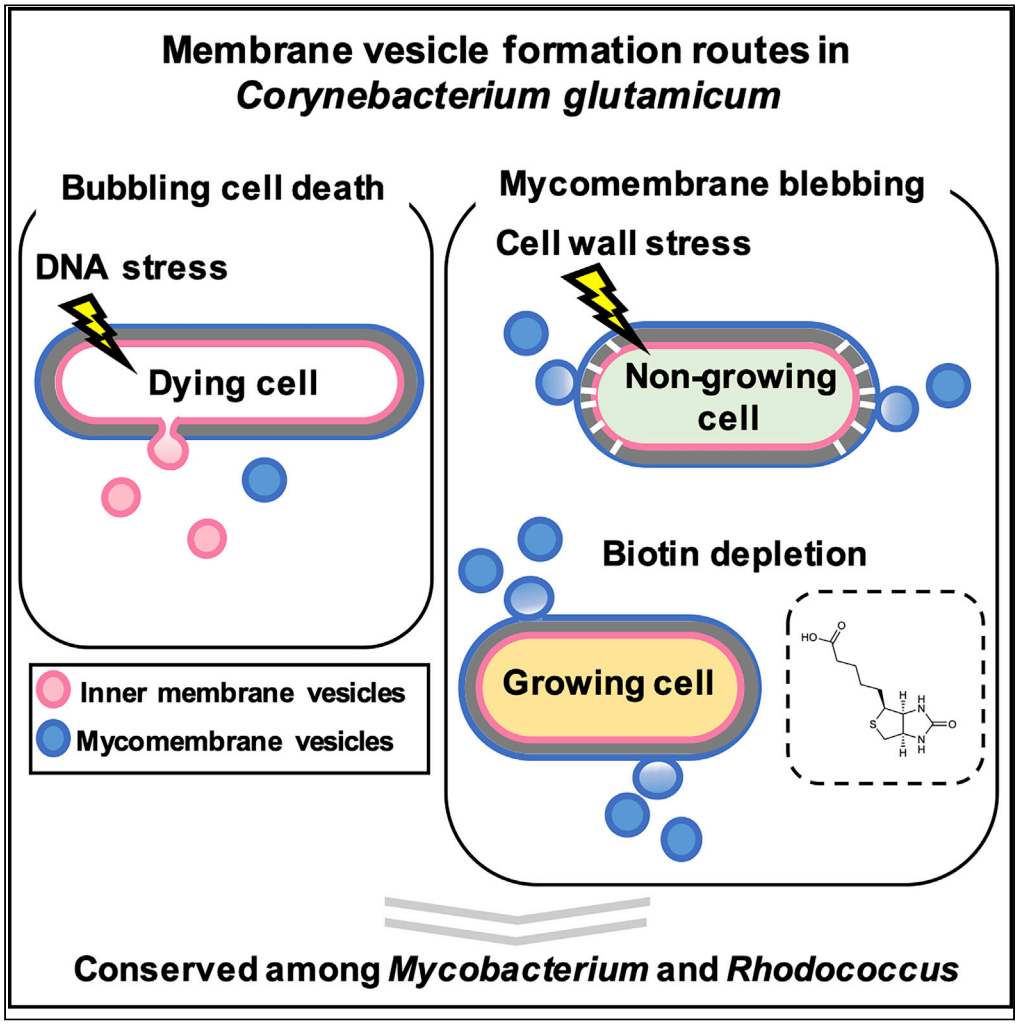

Toshiki Nagakubo, Yuhei O. Tahara, Makoto Miyata, Nobuhiko Nomura, Masanori Toyofuku

nomura.nobuhiko.ge@u.tsukuba.ac.jp (N.N.)
toyofuku.masanori.gf@u.tsukuba.ac.jp (M.T.)

HIGHLIGHTS

Distinct types of MVs are formed in bacteria with complex cell envelopes

MVs can be formed from growing and dying cells via different routes

Unique multivesicular MVs can be formed

The MV formation routes are conserved among several mycolic-acid containing bacteria

Nagakubo et al., iScience 24, 102015
January 22, 2021
https://doi.org/10.1016/j.isci.2020.102015

iScience

CellPress
OPEN ACCESS

Article

Mycolic acid-containing bacteria trigger distinct types of membrane vesicles through different routes

Toshiki Nagakubo,[1,2] Yuhei O. Tahara,[3,4] Makoto Miyata,[3,4] Nobuhiko Nomura,[1,5,*] and Masanori Toyofuku[1,5,6,*]

SUMMARY

Bacterial membrane vesicles (MVs) are attracting considerable attention in diverse fields of life science and biotechnology due to their potential for various applications. Although there has been progress in determining the mechanisms of MV formation in Gram-negative and Gram-positive bacteria, the mechanisms in mycolic acid-containing bacteria remain an unsolved question due to its complex cell envelope structure. Here, by adapting super-resolution live-cell imaging and biochemical analysis, we show that *Corynebacterium glutamicum* form distinct types of MVs via different routes in response to environmental conditions. DNA-damaging stress induced MV formation through prophage-triggered cell lysis, whereas envelope stress induced MV formation through mycomembrane blebbing. The MV formation routes were conserved in other mycolic acid-containing bacteria. Our results show how the complex cell envelope structure intrinsically generates various types of MVs and will advance our knowledge on how different types of MVs can be generated from a single cell organism.

INTRODUCTION

Most bacteria form membrane vesicles, which play important roles in various biological processes (Schwechheimer and Kuehn, 2015) such as bacterial communication (Toyofuku et al., 2017b), resistance to antibiotics and phages (Manning and Kuehn, 2011), and immunomodulation of the host (Vidakovics et al., 2010). Due to these various biological functions and their great potential for application in biotechnology, such as the development of vaccines (Robbins and Moreli, 2014) and drug delivery vehicles (Gujrati et al., 2014), MVs have been attracting attention of researchers in broad areas of life science and biotechnology and the understanding of MV formation mechanisms are fundamental. MVs were classically thought to be formed by the blebbing of the outer membrane in Gram-negative bacteria and therefore were called outer membrane vesicles (OMVs). Outer membrane blebbing is caused by either unbalanced cell envelope biosynthesis or the intercalation of hydrophobic molecules into the outer membrane (Schwechheimer and Kuehn, 2015). In addition, it was recently shown that a Gram-negative bacterium, *Pseudomonas aeruginosa*, can form MVs through explosive cell lysis that is triggered by the expression of peptidoglycan-degrading enzyme, endolysin, encoded in a cryptic phage region (Turnbull et al., 2016). Explosive cell lysis is a process where endolysin degrades the peptidoglycan, resulting in cells lysis with shattered cellular membrane fragments subsequently rounding up and forming MVs (Toyofuku et al., 2019; Turnbull et al., 2016). Endolysin also triggers MV formation in Gram-positive bacteria, such as *Bacillus subtilis* (Toyofuku et al., 2017a) and *Staphylococcus aureus* (Andreoni et al., 2019), but through a distinct process as the cell morphology stays intact due to the thick cell wall. This process is named bubbling cell death (Toyofuku et al., 2019) where endolysin initially forms holes in the cell wall through which membrane protrudes and forms cytoplasmic membrane vesicles (CMVs) (Toyofuku et al., 2019). In contrast to the progress made for Gram-negative and Gram-positive bacteria, the mechanism of MV formation in mycolic acid-containing bacteria (MCB) remains poorly understood.

A main reason why MV formation is not well understood in MCB is due to their complex cell structure. MCB include industrially and clinically important species of *Rhodococcus* and *Mycobacterium*, such as *Mycobacterium tuberculosis* (Prados-Rosales et al., 2011), and are characterized by their unique lipid-rich cell envelope structures. MCB possess a mycomembrane (Dulberger et al., 2020), outside of the thick cell wall, which mainly consists of mycolic acids (Figure 1A). The mycomembrane confers immunomodulatory functions

[1]Department of Life and Environmental Sciences, University of Tsukuba, Tsukuba, Japan

[2]Current affiliation: Graduate School of Agricultural and Life Sciences, The University of Tokyo, Tokyo, Japan

[3]Graduate School of Science, Osaka City University, Osaka, Japan

[4]The OCU Advanced Research Institute for Natural Science and Technology (OCARINA), Osaka City University, Osaka, Japan

[5]Microbiology Research Center for Sustainability (MiCS), University of Tsukuba, Tsukuba, Japan

[6]Lead contact

*Correspondence: nomura.nobuhiko.ge@u.tsukuba.ac.jp (N.N.), toyofuku.masanori.gf@u.tsukuba.ac.jp (M.T.)

https://doi.org/10.1016/j.isci.2020.102015

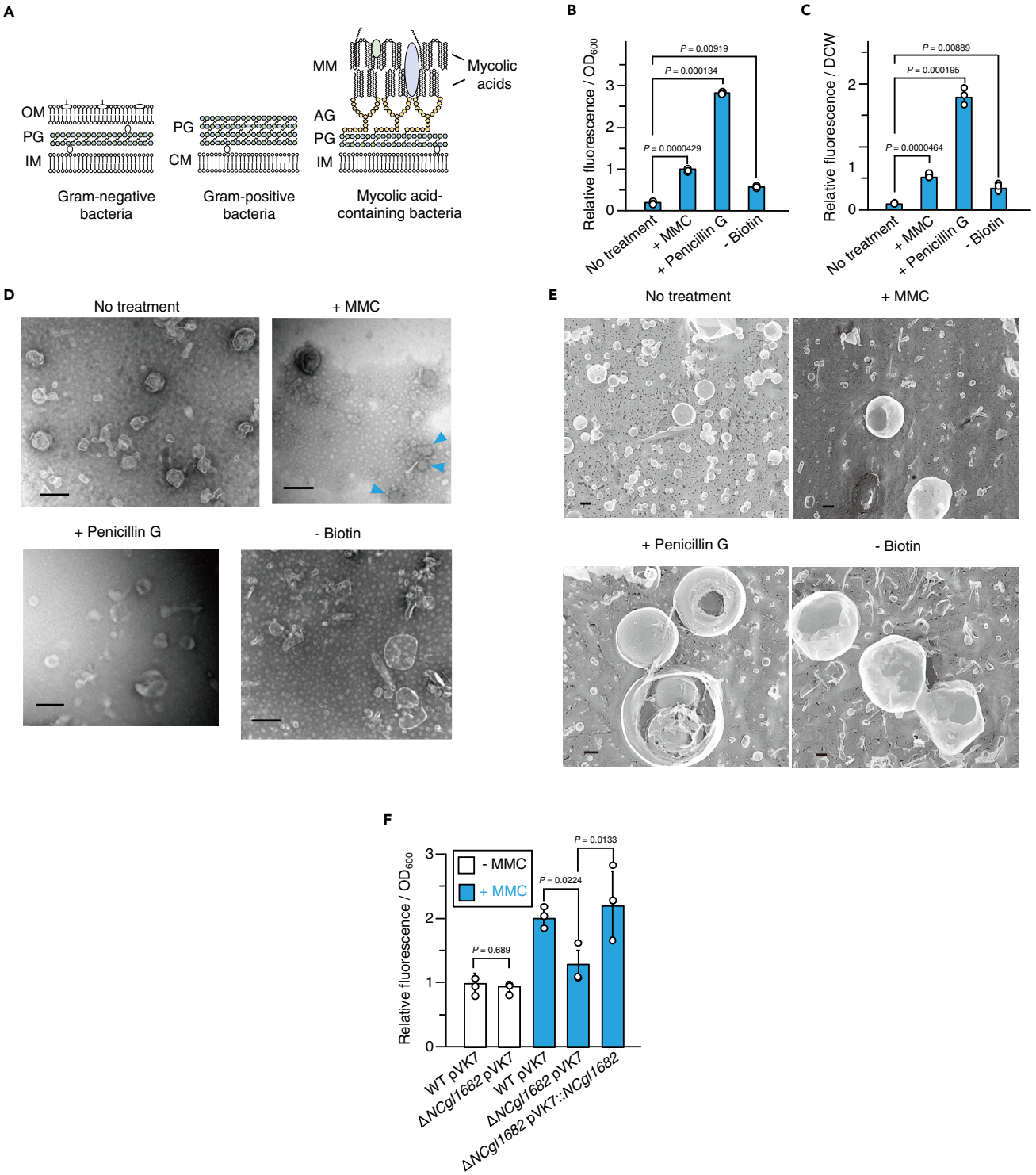

Figure 1. Induction of membrane vesicle formation in *Corynebacterium glutamicum*

(A) Structures of the cell envelope of Gram-negative (left), Gram-positive (middle), and mycolic acid-containing bacteria (right). OM, outer membrane; MM, mycomembrane; PG, peptidoglycan; IM, inner membrane; and AG, arabinogalactan; CM, cytoplasmic membrane.

(B and C) Membrane vesicle (MV) release by *C. glutamicum* under MV formation-inducing conditions. FM4-64 fluorescence of the purified MV fractions was normalized to (B) OD_{600} or (C) dried cell weight (DCW). All values indicated by the bars represent the mean value ± SD for three experiments. p values were calculated using unpaired t test with Welch's correction.

Figure 1. *Continued*
(D) Transmission electron microscopic (TEM) images of MVs released by *C. glutamicum* under the conditions shown in (B and C). Scale bars, 200 nm. Structures that are presumably MVs collapsed are indicated with blue arrowheads.
(E) Quick-freeze deep-etch (QFDE) electron microscopic images of MVs. Scale bars, 200 nm.
(F) MV release by wild-type *C. glutamicum* and *NCgl1682* deletion mutant. White and blue bars indicate the presence or absence of MMC in the culture media, respectively. All values indicated by the bars represent the mean value ± SD for three experiments. p values were calculated using unpaired t test with Welch's correction.

and remarkable tolerance against antimicrobials (Brennan and Nikaido, 1995) and organic solvents (Fernandes et al., 2003), enabling MCB to adapt to various niches.

Recent studies have reported that *Mycobacterium* species form MVs that have immunomodulating activity and iron-acquisition function (Prados-Rosales et al., 2011, 2014). For example, *Mycobacterium tuberculosis* and *Mycobacterium bovis* bacille Calmette-Guérin (BCG) have been shown to release MVs, which can induce an inflammatory response in mice lung in a TLR2-dependent manner (Prados-Rosales et al., 2011). Iron-deficient condition induced the release of siderophore-rich MVs in *M. tuberculosis*, suggesting a role of *M. tuberculosis* MVs in iron-acquisition for survival of the bacterium in host animal (Prados-Rosales et al., 2014). Although these observations have important implications on the biological significance of MVs in MCB, how MVs are triggered and formed in MCB remains a big question. Previous studies (Prados-Rosales et al., 2011, 2014) show *Mycobacterium* MVs form inner membrane vesicles (IMVs), further questioning the mechanisms of how they can traverse the cell wall and the mycomembrane. In addition, despite the presence of the mycomembrane in the MCB cells, MVs derived from the mycomembrane are scarcely reported and their formation mechanisms are largely unknown (Wang et al., 2020).

Here we show that the formation of two distinct types of MVs, namely, mycomembrane vesicle (mMV) and IMV, are induced in MCB due to different types of stress, such as DNA damaging stress, cell wall synthesis inhibition, or fatty acid biosynthesis inhibition (biotin depletion), which resemble the stress bacteria are exposed to in natural settings and have clinical significance (Carfrae et al., 2020; Hayashi et al., 2017; Kümmerer, 2003; Larsson, 2014; Park et al., 2011; Schaefer et al., 1955; Stallings and Glickman, 2010).

To understand how MCB form MVs in details, we examined MV formation in *Corynebacterium glutamicum* as a model organism. *C. glutamicum* is one of the most studied MCB and is a major player in the industrial production of valuable biomolecules such as glutamate. The cell envelope of *C. glutamicum* consists of an inner membrane, peptidoglycan, arabinogalactan, and a mycomembrane rich in corynomycolic acids (C32–C36 fatty acids; Figure 1A) (Bukovski, 2013; Hashimoto et al., 2006).

Using quick-freeze deep-etch electron microscopy (QFDE) and super resolution live cell imaging, we show that *C. glutamicum* MVs show different morphology and mode of formations depending on the inducing condition, and we further characterized the origin of each type of MVs by examining their lipid and protein compositions. Our results reveal that the complex envelope structure of *C. glutamicum* integrates the MV formation processes of both Gram-negative and Gram-positive bacteria, resulting in the generation of MVs with different origins through blebbing of the mycomembrane and bubbling cell death. These mechanisms were conserved in several MCB tested that have clinical relevance and may provide a platform for MV applications such as vaccine development. We also show that the localized site from which MVs are formed, such as cell poles, influence the MV composition, implying that the heterogeneous distribution of lipids and proteins in the membrane (Matsumoto et al., 2006; Toledo et al., 2018) may lead to generate heterogeneous MVs (Kikuchi et al., 2020). Although bacteria are thought as relatively simple single cell organisms and MVs formed from them are thought to be as simple, our finding provides basic knowledge on the different mechanisms of generating different types of MVs.

RESULTS

DNA-damaging stress induces MV formation in *C. glutamicum*

Given the general role of DNA-damaging stress in MV formation of Gram-negative and Gram-positive bacteria ((Toyofuku et al., 2017a); Turnbull et al., 2016), we first investigated whether DNA-damaging stress would trigger MV formation in *C. glutamicum*. To evaluate the involvement of DNA damage, we treated *C. glutamicum* with mitomycin C (MMC), which is a genotoxic compound widely used in inducing DNA damage (Frunzke et al., 2008; Nanda et al., 2014). *C. glutamicum* ATCC13032 was grown to early

exponential phase in the minimum medium (MM-1) as described in the Methods, and MMC was then added to the culture medium to a final concentration of 100 ng mL^{-1}. After 12-h incubation, MVs were purified from the culture medium by density gradient ultracentrifugation, analyzed by nanoparticle tracking (Figure S1), and quantified using FM4-64, which stains the membrane. MV release increased in the MMC-treated cells compared with that of the control cells (Figures 1B, 1C, and S2).

MVs induced with MMC (M-MVs) were investigated using transmission electron microscopy (TEM) and were shown to be more diverse in morphology (spherical, tube-like, and shrunken) and in sizes than MVs formed under normal conditions (N-MVs) (Figure 1D). The ultrastructure of MVs was further investigated using QFDE that allows to observe the native structure of the samples at 1 nm resolution (Tulum et al., 2019). The spherical structures were also confirmed using QFDE and showed wrinkling of the surface and lipid bilayer structures (Figures 1E and S3). In addition, tube-like vesicle structures were occasionally observed in MVs induced under MMC conditions (M-MVs; Figures 1D and 1E).

DNA damage is shown to induce MV formation through the expression of peptidoglycan-degrading enzymes, endolysin, which are usually encoded in prophage regions of the genome (Andreoni et al., 2019)((Toyofuku et al., 2017a); Turnbull et al., 2016). *C. glutamicum* ATCC13032 possess three prophages (CGP1, CGP2, and CGP3) in its genome with a functional endolysin (NCgl1682) being encoded in CGP3 (Frunzke et al., 2008). When *NCgl1682* was deleted, M-MV formation was not triggered by MMC, but could be restored by *NCgl1682* complementation under control of its native promoter (Nanda et al., 2014) (Figure 1F). These results showed that MMC triggered MV formation through NCgl1682, further demonstrating the universal role of endolysin in MV formation.

Endolysin triggered MV formation through cell death

Endolysin is known to trigger explosive cell lysis in Gram-negative bacteria or bubbling cell death in Gram-positive bacteria ((Toyofuku et al., 2017a); Turnbull et al., 2016). In explosive cell lysis, the cells "explode," resulting in the shattered membrane to round up and form MVs, whereas in bubbling cell death MVs initially protrude from structurally intact cells. To understand the MV formation process in *C. glutamicum*, we performed super resolution live-cell imaging using confocal laser scanning microscopy (CLSM) with Airyscan detector. MV formation was observed from cells that were structurally intact (Figure 2A; Video S1). However, staining of cells with a membrane-impermeable dye (SYTOX green) indicated that the MV-forming cells had impaired membranes, similar to what has been observed in bubbling cell death of *B. subtilis* (Figure 2A; Video S1) (Toyofuku et al., 2017a).

None of the MV-forming cells divided further during approximately 5 h of observation (Figure S4). This suggested that the cells died upon MV formation. Thin-section TEM and scanning electron microscopic (SEM) images confirmed that many MVs were associated with the surface of MMC-treated cells and were less electron dense in TEM compared with that of the untreated cells, suggesting cytoplasmic content had been released (Figures 2B, 2C, and S5).

Cell envelope stress induced MV formation through blebbing of mycomembrane

Previous studies of Gram-negative bacteria have suggested that an imbalance of membrane and peptidoglycan synthesis eventually leads to outer membrane blebbing that pinches off to form MVs (Toyofuku et al., 2019)(Sutterlin et al., 2016). As MCB possess mycomembranes oustide the cell wall, we examined whether alterations in cell envelope synthesis would lead to MV release in *C. glutamicum*. To this end, we used penicillin G treatment and biotin-deficient conditions, which are reported to alter the cell envelope structure by inhibiting cell wall biosynthesis or fatty acid biosynthesis, receptively, in *C. glutamicum* (Hoischen and Kraman, 1990; Nakayama et al., 2018). *C. glutamicum* was grown to early exponential phase in MM-1 medium, and then a sub-lethal concentration of penicillin G (0.4 U mL^{-1}) was added to the culture. The penicillin G treatment of *C. glutamicum* induced MV release (Figures 1B–1D, S1, and S2). Interestingly, QFDE revealed that P-MVs (penicillin G-induced MVs) were usually internally packed with small MVs and chains of MVs, resulting in distinct structures compared with those of other types of MVs (Figure 2D). To determine the influence of biotin deficiency, which consequently decreases total amount of membrane lipids and alters membrane composition in the bacterium (Hoischen and Kraman, 1990; Nakayama et al., 2018), *C. glutamicum* cells were grown in biotin-deficient MM-1 medium (1 μg L^{-1} biotin). MV release was significantly increased under biotin-deficient conditions compared with that of biotin-sufficient conditions (100 μg L^{-1} biotin), indicating that biotin deficiency induced MV release in *C. glutamicum* (Figures 1B,

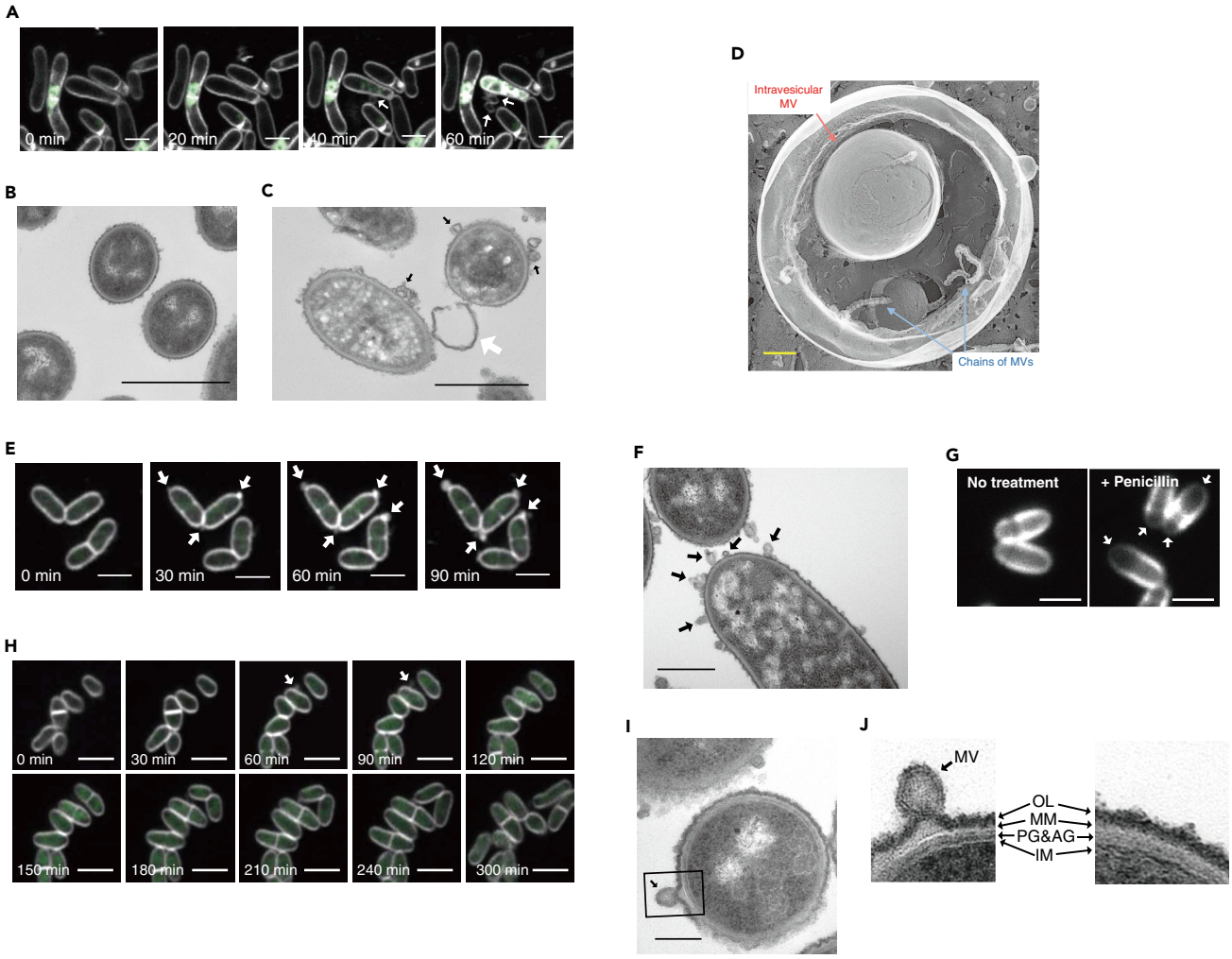

Figure 2. MV release by *Corynebacterium glutamicum* via different routes

(A, E, and H) Live-cell imaging of MV formation of *C. glutamicum* under (A) MMC condition, (E) penicillin G, and (H) biotin-deficient conditions. The image shows FM4-64 (white) merged with SYTOX green (green). Movies are shown as Videos S1, S2, and S3. White arrows indicate MVs. Scale bars, 2 μm.

(B and C) Thin-section TEM images of *C. glutamicum* cells under (B) no treatment and (C) MMC conditions. Black and white arrows indicate MVs and presumably a cell wall fragment, respectively. Scale bars, 1 μm.

(D) Magnified QFDE image of MVs formed under penicillin G treatment condition. Red arrow and blue arrows indicate intravesicular MV and chains of MVs, respectively. Scale bar, 200 nm.

(F) Thin-section TEM images of *C. glutamicum* cells under penicillin G. Black arrows indicate MVs. Scale bar, 1 μm.

(G) Peptidoglycans of *C. glutamicum* cells were visualized using HADA in the presence or absence of penicillin G. White arrows indicate the cell pole in which peptidoglycan synthesis is severely inhibited by penicillin G treatment. Scale bars, 2 μm.

(I) Thin-section TEM images of *C. glutamicum* cells under biotin-deficient conditions. Scale bar, 200 nm.

(J) Magnified images of the cell envelope of an MV-forming cell (left, black square in I) and a non-forming cell (right). OL, outer layer; OM, outer membrane; PG, peptidoglycan; AG, arabinogalactan; IM, inner membrane.

1C, S1, S2, and S5). Purified B-MVs (biotin deficiency-induced MVs) exhibited spherical and tube-like structures under TEM and QFDE, and tube-like MVs were observed more frequently than N-MVs and P-MVs (Figures 1D and 1E). It is well known that in *C. glutamicum* biotin deficiency and penicillin G treatment induce glutamate efflux through NCgl1221, a mechanosensitive channel (Nakamura et al., 2007; Nakayama et al., 2018; Nara et al., 1964; Shiio et al., 1962). The amount of glutamate or lysine contained in each purified MV fraction accounted for 0.015%–0.05% of the total glutamate or lysine content in the culture supernatant (Figures S6 and S7), indicating that glutamate and lysine were primarily released into the supernatant through NCgl1221, but not via MVs.

Penicillin G induced MV formation in the cell pole of *C. glutamicum*

Different from MMC-treated cells, penicillin G-treated cells formed MVs from the cell pole (Figures 2E, S5, S8, and S9; Video S2). Cell permeability did not increase in the penicillin-treated cells (Figure 2E; Video S2) and approximately 10% of the MV-forming cells underwent cell division (n = 86; Figures S4 and S8). However, these cells stopped growing after MV release. Thin-section TEM of penicillin-treated cells showed MV blebbing from the cell surface (Figure 2F). As penicillin G inhibits cell wall synthesis, we visualized the effect of penicillin G on the cell wall of *C. glutamicum* using fluorescent labeling of the cell wall with HCC-amino-D-alanine (HADA), a synthetic D-amino acid with a fluorescent side chain (Kuru et al., 2012). The results showed that HADA fluorescence was barely detectable at the cell pole when the cells had been treated with penicillin G. However, HADA fluorescence was uniformly distributed along the cell envelope in the control cells not treated with penicillin G (Figure 2G and S10). These results indicated that penicillin G had more severe effect on the cell pole where cell wall would undergo frequent reorganization, and consequently inhibited cell growth. We assume that the inhibition of the peptidoglycan biosynthesis would make the mycomembrane-peptidoglycan linkage unstable, which would eventually lead to the blebbing of MVs.

Membrane stress by biotin deficiency induces MV formation in growing *C. glutamicum* cells

Under biotin-deficient conditions, over 80% of the MV-forming cells (n = 14) grew and divided after MV formation during the 5-h observation period of the study (Figure 2H and S4; Video S3). We believe this is the first clear evidence of cell division after MV release, supporting a canonical MV blebbing model of MVs being formed during cell growth (Beveridge, 1999). MV formation by *C. glutamicum* under biotin-sufficient conditions was not observed using CLSM due to lower MV formation and faster cell growth compared with that under biotin-deficient conditions. Interestingly, thin-section TEM of cells under biotin-deficient condition revealed protrusions of the cell envelope where B-MVs were observed (Figures 2I and 2J). These protrusions were observed with significantly higher frequency at the sites of MV formation than in the sites where no MV formation was observed (Figure S11), whereas the protrusions were seldomly observed on cells grown under normal conditions (Figure 2B). These results suggest that an imbalance in the synthesis of the cell envelope or accumulation of substances such as proteins may have led to the membrane protrusions that formed the MVs.

MV lipid composition indicates different origins of MVs

Live-cell imaging indicated that *C. glutamicum* was able to form MVs through different process under different conditions. This led to our hypothesis that MVs may differ in their composition. Therefore, MV lipid content of different types of MVs, including MVs isolated from culture without any treatment (N-MVs), was analyzed using gas chromatography/mass spectrometry (GC/MS) and liquid chromatography/mass spectrometry (LC/MS). Corynomycolic acids (CMs) (Bukovski, 2013; Hashimoto et al., 2006), which are major components of *C. glutamicum* mycomembrane (Figure 1A), were detected in all types of MVs (Figures 3A and S12). This provided a general feature of MVs released from this bacterium. Most of the CMs detected were trehalose dicorynomycolic acids (TDCMs), which are found in the outer leaflet of the CM bilayer and are not covalently bound to the cells' arabinogalactan (Figures S12–S14) (Bukovski, 2013). To gain more insight into the origins of *C. glutamicum* MVs, we extracted mycomembrane and inner membrane lipids separately from *C. glutamicum* cell (described under Methods). The selectivity of the membrane lipid separation is supported by the observation that the mycomembrane extracts were apparently colorless, whereas the inner membrane extracts were yellow-pigmented, indicating the presence of renoxanthin (a C_{50} carotenoid), which localizes in the inner membrane (Sandmann ans Yukawa, 2005). We then separated and detected the major lipids from each membrane and MV fractions by thin-layer chromatography (TLC; Figure S15) and compared the intensity ratios of TDCMs/phospholipids (Figure 3B). Overall, the intensity ratios of TDCMs/phospholipids were higher in MVs than in the inner membrane fraction, suggesting that the MVs contained lipid components of the mycomembrane. However, a comprehensive analysis and comparison of the lipid composition among the mycomembrane, inner membrane, and MVs (Figures S16–S18; described under Methods) showed that the N-MVs fraction, P-MVs fraction, and B-MVs fraction had more similar composition to the mycomembrane than that to the inner membrane fraction, whereas M-MVs fraction had lipid composition more similar to that of the inner membrane fraction (Figures 3C and S16–S18). Most remarkably, P-MVs fraction contained most of the mycomembrane-specific lipids (7 of 9) but none of the inner membrane-specific lipids (Figures 3C and S16–S18). The presence of inner membrane lipids in N-MVs and B-MVs fractions may be due to the formation of IMVs resulting from the basal level of cell death in cell cultures, whereas presence of IMVs was overcovered by mMVs in case of P-MVs. Notably, the lipid profile of N-MVs fraction was different from those of M-MVs, P-MVs, and B-MVs fractions (Figures S16–S18),

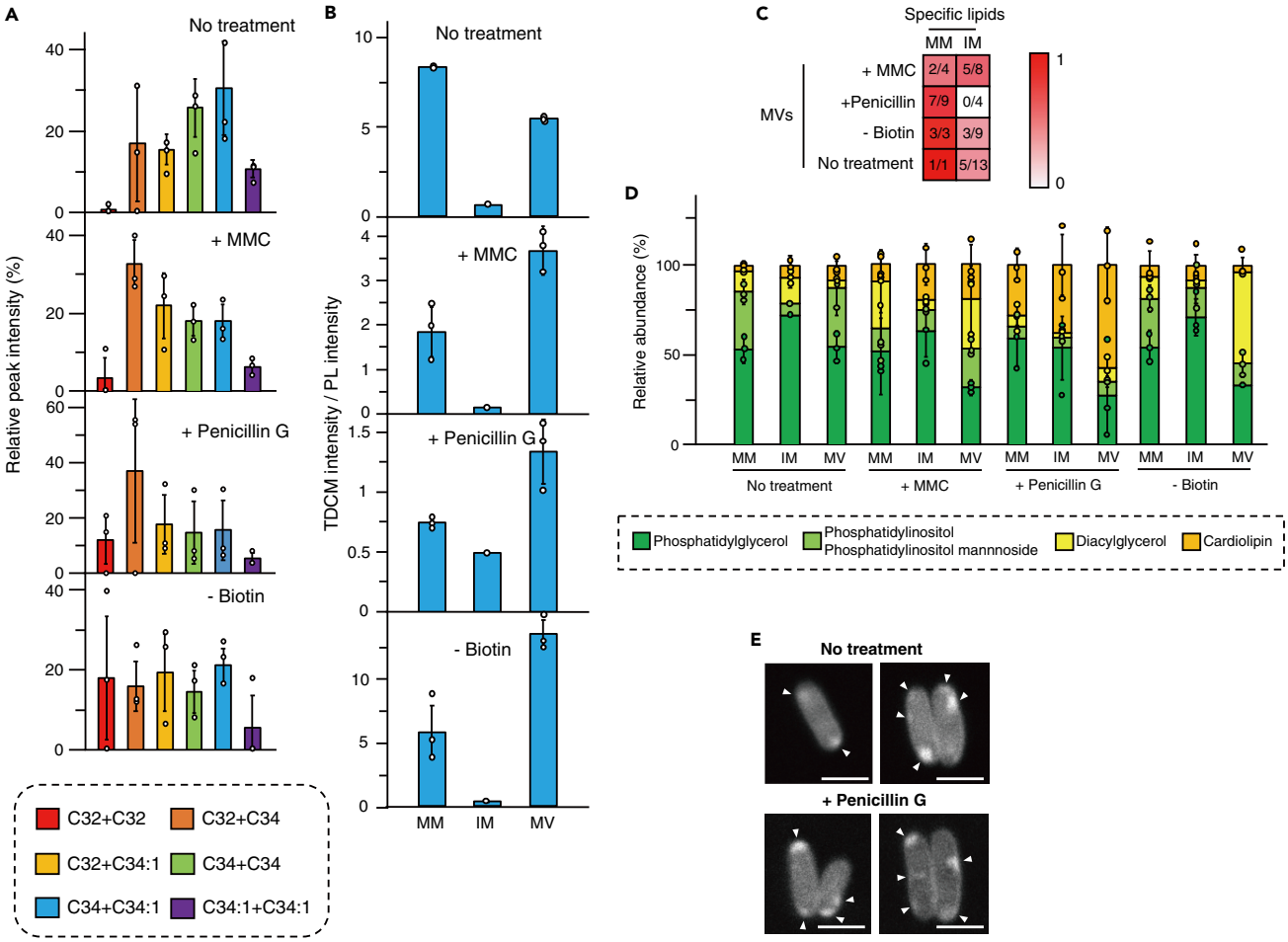

Figure 3. Lipid compositions of MVs

(A) Trehalose dicorynomycolic acids (TDCMs) were detected from MVs using LC/MS. The structure of each TDCM was determined based on the results of GC/MS and LC/MS/MS analyses shown in Figures S12 and S14.

(B) Intensities of TDCM and phospholipids (PLs) in TLC analysis were compared using ImageJ. Each lipid was extracted from mycomembrane (MM), inner membrane (IM), and MV of *Corynebacterium glutamicum*, and then separated by TLC as described under Methods. All values indicated by the bars represent the mean value ± SD for three experiments.

(C) Mycomembrane-specific lipids (MMSLs) and inner membrane-specific lipids (IMSLs) of *C. glutamicum* cells under various growth conditions were identified by LC/MS analyses. In these analyses, we defined MMSLs and IMSLs as the lipids that were detected in either the mycomembrane (1-butanol extract) or the inner membrane extract (total of chloroform/methanol and chloroform/methanol/water extracts) of *C. glutamicum* cell under each of the designated culture conditions. Detailed information of these analyses is shown in Methods and Figures S15–S18. Denominator of each fraction indicates total number of specific lipids in the mycomembrane or the inner membrane extract of *C. glutamicum* cells under different culture condition, and the numerator of each fraction indicates total number of those MMSLs or IMSLs detected in MVs.

(D) Lipid compositions of mycomembrane, inner membrane, and MVs were analyzed. Mycomembranes and inner membranes were extracted separately from cells using 1-butanol and chloroform/methanol solutions, respectively. Lipids were quantified using TLC and standard lipids. All values indicated by the bars represent the mean value ± SD for three experiments.

(E) Cardiolipins were visualized using acridine orange 10-nonyl bromide. White arrowheads indicate the localization of cardiolipins. Scale bars, 2 μm.

and the addition of biotin to the culture failed to decrease N-MV release (Figure S19), indicating that N-MVs were formed through a mechanism different than that of B-MVs. The drastic changes in the cellular membrane lipid compositions among the growth conditions, especially MMC and penicillin G conditions, suggest stress-responsive membrane remodeling caused by MalR (Hünnefeld et al., 2019), a MarR-type regulator that has been proposed to be involved in adaptation of *C. glutamicum* cells to DNA stress and inhibition of cell wall biosynthesis. The previous study (Hünnefeld et al., 2019) has identified binding sites of MalR in *C. glutamicum* genomes and revealed that MalR regulates expressions of several genes, such as *ipsA* and *oppA*, involved in cell membrane remodeling. Positive and negative regulation of these genes by

MalR may result in modulation of lipid composition of *C. glutamicum* membranes upon the cell envelope and DNA stresses.

To determine whether the presence of mycomembrane was essential for the induction of MV formation, we constructed a Δ*pks13* mutant of *C. glutamicum*, which lacked corynomycolic acids and a mycomembrane (Portevin et al., 2004; Zuber et al., 2008). This mutant exhibited less MV release than that of the wild-type strain under normal growth conditions (Figure S20). Moreover, MV release tends to be induced with MMC treatment of the mutant, but not with biotin deficiency or penicillin G treatment (Figure S20). This further indicates that outer membrane is essential for the induction of MV release in *C. glutamicum* under the latter two envelope stress conditions, whereas IMVs formation can be trigged by degradation of the cell wall in the mutant cells.

Comparison of the lipid groups showed that the ratios of phosphatidylglycerol (PG), phosphatidylinositol, diacylglycerol (DG), and cardiolipin (CL) differed depending on the MVs (Figures 3D and S15). The conical shape of DG is reported to form a negative curvature in membranes, which supports budding in eukaryotes (Agrawal and Ramachandran, 2019). We found that DG was enriched in B-MVs fraction, implying a similar role in MV formation under biotin-deficient conditions. CL is another conical-shaped lipid and was found to be enriched in P-MVs fraction (Figures 3D and S15). CL consists of two PGs that are linked by a glycerol head group and are major membrane components in bacteria and mitochondria (Mileykovskaya and Dowhan, 2009). CL has been found to accumulate at the cell pole (Mileykovskaya and Dowhan, 2000) and at curved regions of membranes (Renner and Weibel, 2011) of bacteria, suggesting that the clustering of CL may cause membrane curvature in bacterial membranes, and may also lead to the formation of MV chains. Cell imaging showed that CL tended to localize at the cell pole of *C. glutamicum* (Figure 3E), consistent with our results of penicillin G treatment leading to MV formation in the cell pole (Figures 2E and 2F). In addition, CL content was high in the cell membrane of penicillin G-treated cells (Figure 3D), suggesting that the treatment led to remodeling of the membrane composition. Given that expression of CL synthase (NCgl2646) has been reported to be elevated upon penicillin G treatment in *C. glutamicum* (Hirasawa et al., 2018), the higher CL content in the penicillin G-treated cells may be due to increased *de novo* biosynthesis of CL. In addition, cell wall-associated CL, which is not extractable from the cells under normal growth condition (Bansal-Mutalik and Nikaido, 2011), may be released upon cell wall damaging by penicillin G and localize in cell membrane as extractable lipid.

M-MVs, but not other MVs, included cytoplasmic substances

Many MVs have been shown to carry cytoplasmic materials such as DNA as cargo, and it has been proposed that MVs blebbing from the outer membrane do not contain cytoplasmic material, whereas MVs generated through cell lysis or cell death contain cytoplasmic material in their cargo (Toyofuku et al., 2019). To better understand the origins of MVs, we quantified the amount of double-stranded DNA (dsDNA) in the MVs. The results clearly demonstrated that dsDNA was most abundant in the M-MVs and was scarcely detected in the other types of MVs (Figure 4A). In addition, we conducted mass spectrometric analysis to identify proteins enriched in the MVs. Proteins in MVs were separated by gel electrophoresis, and the major proteins were subjected to mass spectrometry (details are described under Methods). Consistent with the result of DNA quantification, cytosolic proteins 5-methyltetrahydropteroyltriglutamate-homocysteine *S*-methyltransferase and elongation factor Tu and inner membrane protein ATP synthase β-subunit were abundant in M-MVs, but not detected in the other MVs (Figure 4B). Surprisingly few protein bands were detected by SDS-PAGE analysis of N-MVs and P-MVs (Figures 4B and S21). NCgl0381 is a hypothetical membrane protein containing a predicted N-terminal secretion signal peptide sequence and was predominantly detected in N-MVs (Figures 4B and S22). The most abundant protein in P-MVs was PS1, a mycoloyl transferase that is involved in the biosynthesis of TDCMs (Puech et al., 2000). PS1 is associated with the cell envelope and also secreted into the culture medium (Brand et al., 2003). Furthermore, corynomycoloyl transferase C chain A (Cmt1) and esterase family protein (Cmt2), which are involved in the biosynthesis of TDCM and localize in the cell envelope (Brand et al., 2003), were detected in B-MVs (Figure 4B). CspB, which was previously reported to be abundant in MVs induced by EDTA treatment of *C. glutamicum* ATCC13869 (Theresia et al., 2018), was not detected in MVs analyzed in the current study due to the absence of this protein in the strain we used (Yang and Yang, 2017). These results support the idea that N-MVs, P-MVs, and B-MVs were primarily formed through mycomembrane blebbing, whereas M-MVs were formed through bubbling cell death, which leads to inner membrane protrusion and liberation of the mycomembrane due to cell wall degradation.

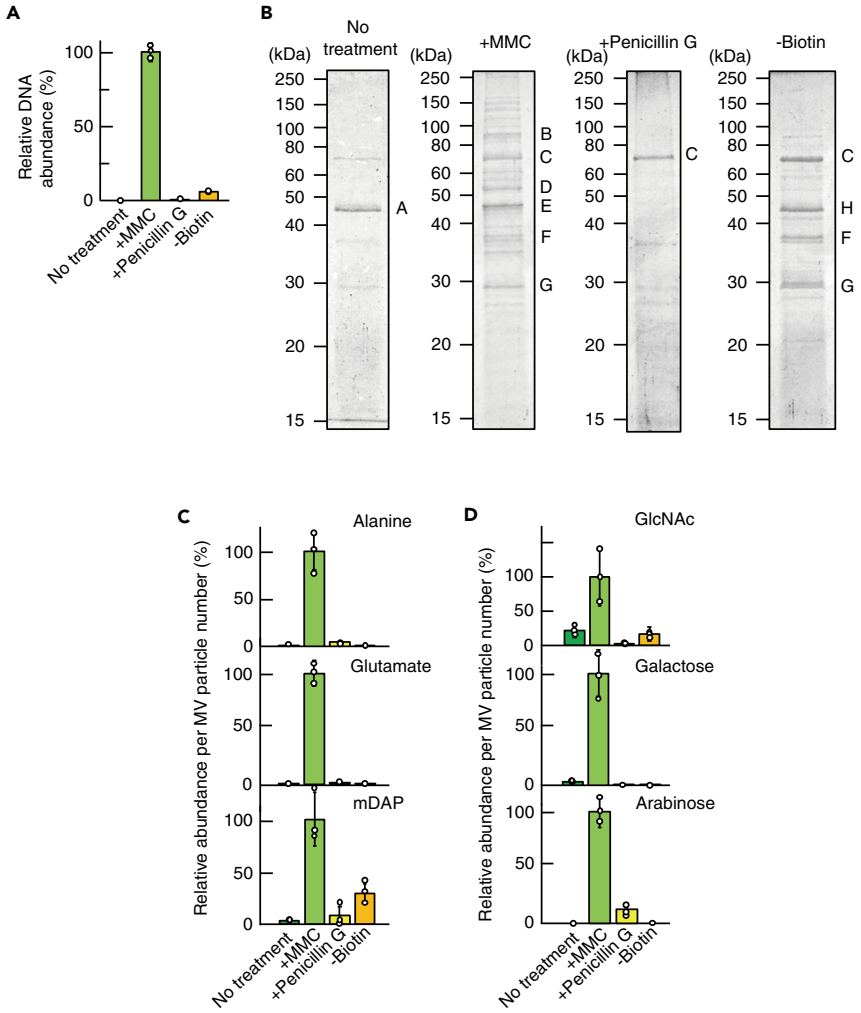

Figure 4. Detection of various cellular components in MVs

(A) Quantification of concentrations of double-stranded DNA associated with *C. glutamicum* MVs. All values indicated by the bars represent the mean value ± SD for three experiments.

(B) Protein profiles of MVs. A, hypothetical membrane protein (NCgl0381); B, 5-methyltetrahydropteroyltriglutamate-homocysteine *S*-methyltransferase; C, PS1; D, ATP synthase β-subunit; E, elongation factor Tu; F, corynomycoloyl transferase C chain A (Cmt1); G, esterase family protein (Cmt2); H, PS1 fragment. Five micrograms of protein was applied to each lane.

(C and D) Detection and quantification of (C) amino acids and (D) sugars that are derived from cell wall fragments in MVs. All values indicated by the bars represent the mean value ± SD for three experiments.

Cell wall components were associated with M-MVs

Cell wall components, such as peptidoglycan, are typical MV cargo that have important roles in host immune modulation including *M. tuberculosis* (Kaparakis-Liaskos and Ferrero, 2015; Prados-Rosales et al., 2011). However, the process of how the cell wall components are packaged into MVs is not fully understood. In *C. glutamicum*, the major peptide units in the cell wall are L-Ala-D-Glu-*meso*-diamiopimelate (mDAP)-D-Ala and L-Ala-D-Glu-mDAP, which are peptide units cross-linked via mDAP-mDAP bridges (Bukovski, 2013). In addition to these amino acids, *N*-acetylglucosamine (a component of the peptidoglycan backbone) and arabinose and galactose (components of arabinogalactan) are contained in the cell wall (Bukovski, 2013). These molecules were most abundant in M-MVs and scarcely detected in the other types of MVs, further suggesting that cell wall components were packaged into MVs in *C. glutamicum* by degradation of the cell wall (Figures 4C, 4D, and S23). In addition, the molar ratios of Ala/Glu/mDAP were approximately 1.4/1/0.015 in M-MVs compared with approximately 1.4/1/1 in the cells (Figure S24). This suggested that mDAP-mDAP bridges in the peptide units were hydrolyzed by endolysin.

Induction of MV formation among mycolic acid-containing bacteria

As MCB share cell envelope structural features (Figure 1A), we investigated whether MV formation was also induced in *Mycobacterium* and *Rhodococcus* species by biotin deficiency, MMC treatment, and/or penicillin G treatment. We found that MV release was induced in *Mycobacterium smegmatis* MC^2155 (Figures 5A–5G), *Rhodococcus erythropolis* PR4 (NBRC100887) (Figures 5H–5N), and *Rhodococcus equi* IFO3730 (Figures 5O and 5T) under the aforementioned conditions. This is also supported by bioinformatic analyses indicating the presence of lytic enzymes in prophages regions of MCB. Genomic search by PHASTER (Arndt et al., 2016) showed that *M. smegmatis* MC^2155 (putative alpha/beta hydrolases, LJ00_07,870 and LJ00_07,930) and *R. erythropolis* PR4 (putative endolysin, RER_22,520) possess prophages encoding putative lytic enzymes in their genome. Although whole genome information of *R. equi* IFO3730 is not available, PHASTER search revealed that the related strain, *R. equi* ATCC33707, also possesses two prophages in its genome and at least one putative endolysin (HMPREF0724_RS24760) is coded in the region. Of note, we cultured *R. equi* in LB medium supplemented with 200 $\mu g\ L^{-1}$ biotin as MVs in minimum medium was too low to quantify. MV release by *R. equi* significantly increased, even when LB medium was not supplemented with biotin as this medium already contained approximately 1.5 $\mu g\ L^{-1}$ biotin (Figure 5O) (Difco Laboratories, 1998). Size distributions of MCB MVs (Figures 5C–5F, 5J–5M, and 5Q–5S) suggest that the diameter ranges of most of these MVs (approximately 80–200 nm) are similar to those of typical bacterial MVs including previously reported *M. smegmatis* MVs (Prados-Rosales et al., 2011).

DISCUSSION

MV formation has been widely studied in Gram-negative and Gram-positive bacteria, but little is known about MV formation in MCB, which are grouped as Gram-positive bacteria possessing a mycomembrane in addition to a thick cell wall. Previous studies in *Mycobacterium* species have suggested that they mainly form IMVs (Prados-Rosales et al., 2011, 2014), and are induced under iron starvation, which also alters their composition (Prados-Rosales et al., 2014), raising the following fundamental questions: (1) how are IMVs formed and released through the cell wall and the mycomembrane, (2) what causes the change of MV composition under different culture conditions, and (3) how are these MVs induced. Our results show that formation and release of different types of MVs by MCB can be induced through different routes involving the mycomembrane blebbing and bubbling cell death depending on different conditions. Membrane stress or cell wall synthesis inhibition, which presumably leads to the loss of linkage between the cell wall and the mycomembrane, induces mycomembrane blebbing, forming mainly mMVs. Cell wall disruption led to bubbling cell death forming a mixture of mMVs and IMVs. The involvement of cell lysis in MV formation would be one of the mechanisms for IMVs release, and importantly, cytoplasmic and cell wall components were associated with MVs triggered by bubbling cell death.

Distinct routes for MV formation have also been reported in other groups of bacteria. In Gram-negative bacteria, MVs can be formed through blebbing of the outer membrane (Schwechheimer and Kuehn, 2015) or explosive cell lysis (Toyofuku et al., 2019; Turnbull et al., 2016). Bona fide OMVs formed through outer membrane blebbing without cell lysis are suggested to contain limited intracellular components and inner membrane proteins (Toyofuku et al., 2019; Schwechheimer and Kuehn, 2015), whereas MVs formed through explosive cell lysis may contain inner membrane and cytoplasmic materials (Turnbull et al., 2016). In Gram-positive bacteria, MV are formed by alteration or damaging of the cell wall through which the cytoplasmic membrane protrudes and MVs are pinched off (Andreoni et al., 2019)((Toyofuku et al., 2017a); Wang et al., 2018). MV-like particles were observed on the surface of *C. glutamicum* cells under conditions of biotin deficiency (Ochiai et al., 1987) or dysfunction in cell wall biosynthesis (Raad et al., 2010), although they were not characterized at that time. Using super resolution live-cell imaging and biochemical analysis, we showed that lysing *C. glutamicum* cells release IMVs and mMVs through bubbling cell death under MMC treatment condition (Figure 1), and the cells under biotin-deficient condition or penicillin G treatment condition release mMVs through the mycomembrane blebbing without cell lysis (Figure 1). It has been long proposed that OMVs are formed only from growing cells,even though direct evidence using live-cell imaging was lacking (Schwechheimer and Kuehn, 2015). We show that both growing biotin-deficient *C. glutamicum* cells and penicillin G-treated cells release MVs whose compositions indicate their mycomembrane origin, suggesting that mycomembrane blebbing can happen in both dead and alive cells depending on the mechanisms. The involvement of endolysin in MV formation by *C. glutamicum* provides further evidence of its universal role in MV formation among structurally distinct bacteria ((Toyofuku et al., 2017a); Turnbull et al., 2016) and could be a major route for MV formation in natural environments considering their abundance and the numerous mycobacteriophages isolated (Hatfull,

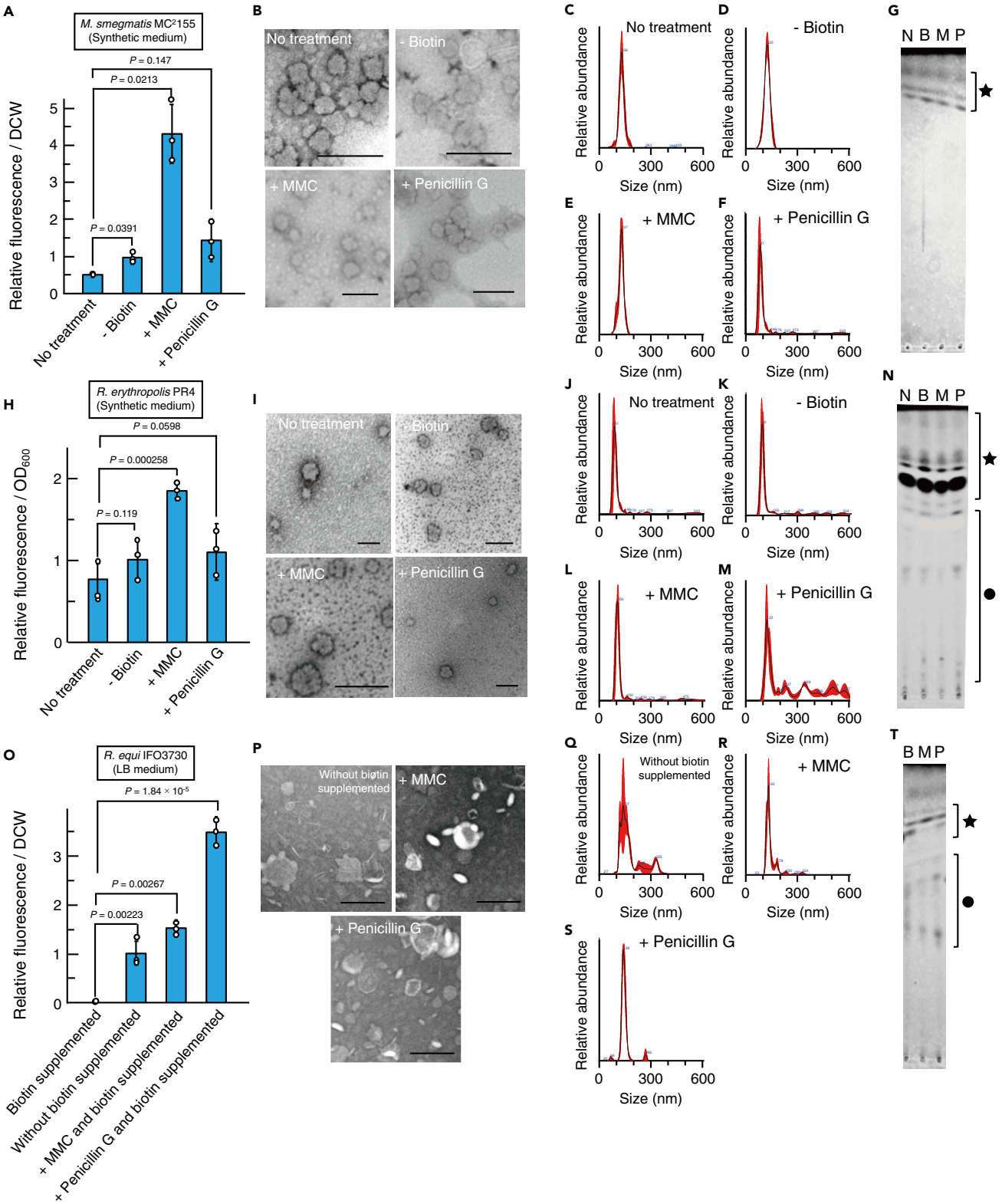

Figure 5. MV induction in other mycolic acid-containing bacteria

(A–T) The panels (A–G, H–N, and O–T) correspond to *Mycobacterium smegmatis* MC^{2}155, *R. erythropolis* PR4, and *Rhodococcus equi* IFO3730, respectively. (A, H, and O) *M. smegmatis*, *R. erythropolis*, and *R. equi* were cultured under various conditions and then their MV release were measured. *M. smegmatis* and

Figure 5. *Continued*

R. erythropolis were cultured in synthetic minimum media, whereas *R. equi* was cultured in LB medium, with and without biotin supplementation, due to extremely low growth in synthetic minimum medium (details of growth conditions are described under Methods). All values indicated by the bars represent the mean value ± SD for three experiments. p values were calculated using unpaired t test with Welch's correction. DCW, dried cell weights. (B, I, and P) TEM images of MVs of the mycolic acid containing bacteria are shown. Scale bars, 200 nm. (C–F, J–M, and Q–S) Particle size distributions of the above MVs. Black lines indicate the mean values of the concentrations of the detected particles in MV solutions. Red regions indicate SD of the mean values. (G, N, and T) Thin-layer chromatography profiles of the above MVs. Lipids were processed using chloroform-methanol-water (65:25:4, v/v). N, no treatment condition; B, biotin-deficient condition in *M. smegmatis* and *R. erythropolis*, or without biotin supplemented in *R. equi*; M, MMC treatment condition; P, penicillin G treatment condition. Black star indicates apolar lipids including mycolic acid esters. Black circle indicates polar lipids including phospholipids.

2018). Although the involvement of bubbling cell death resembles an earlier observation in MV formation in *B. subtilis* (Toyofuku et al., 2017a), it is distinct in that bubbling cell death in *C. glutamicum* also gives rise to mMVs. The MV formation mechanisms characterized in *C. glutamicum* were suggested to be conserved in other MCB tested, including *M. smegmatis*, which has been used as a non-pathogenetic model organism of *M. tuberculosis*, one of the most productive killers among infectious diseases (Smith, 2003). Our results show that due to the rigid cell wall structures and the presence of a mycomembrane in MCB, MV formation in these bacteria reflects the features of both Gram-negative and Gram-positive bacteria, resulting in various MVs being formed with different lipid and protein contents.

Previous studies have shown that lipid and protein profiles often differ between MVs and cellular membrane, suggesting cargo selection during MV biogenesis, whose mechanism is not fully understood (Nagakubo et al., 2020; ; Schwechheimer and Kuehn, 2015). Our study shows that P-MVs formed at the cell pole are enriched in CL and have a different protein profile compared with N-MVs, strongly suggesting that the subcellular localizations of MV formations can generate different type of MVs due to the heterogeneous distribution of lipids and proteins in the membrane. In addition, the accumulation of CL in P-MVs and the cellular membranes under penicillin G condition may also imply its role in MV formation mechanism. Besides CL, B-MVs released under biotin-deficient condition accumulated DG, a minor component of *C. glutamicum* membrane. Notably, CL and DG represent bacterial cone-shaped lipids whose accumulation or sequestration potentially cause membrane curvature (Agrawal and Ramachandran, 2019) and possibly the resultant pinching-off of MVs. It is thus possible that the remodeling of membrane lipid compositions and the enrichment of the cone-shaped lipids in response to the specific growth conditions triggers the membrane budding and the consequent MV formation with the distinct lipid compositions. This is supported by the previous study showing that *Haemophilus influenzae* released OMVs rich in phosphatidylethanolamine (PE), another typical cone-shaped lipid in bacterial membranes, under iron limitation condition (Roier et al., 2016). Together with our results, this and the related study in *Vibrio cholerae* (Zingl et al., 2019) suggest that the remodeling membrane lipid compositions and the accumulation of lipids with certain conformational properties may be a key to understanding a common molecular mechanism underlying MV formation across diverse classes of bacteria.

P-MVs showed a characteristic structure of MVs being packed with smaller MVs, creating multivesicular MVs. How the various MV compositions impact MV morphology is of interest, but currently largely unexplored. Multivesicular structures are observed in biological systems such as multivesicular endosomes, and although the process is not fully understood, the presence of certain lipids and protein complexes are known to play a role in their formation (Matsuo et al., 2004; Trajkovic et al., 2008; Wollert and Hurley, 2010). The unique MV structure of P-MVs may due to the enrichment of CL from the cell pole causing a curvature of the membrane (Agrawal and Ramachandran, 2019; Mileykovskaya and Dowhan, 2000, 2009), rather than a resultant of sample preparation.

In addition, the proteins detected in the current study, PS1 and NCgl0381, which were dominant in P-MVs and N-MVs, respectively (Figure 4B), may potentially be used as a basis for selective compartmentalization of certain proteins using protein fusion to generate specific MVs for various applications in biotechnology, such as purification of heterologously expressed proteins and vaccine development.

Our finding of the involvement of biotin in MV formation has a broad implication. Biotin is an essential biological cofactor involved in key metabolic pathways, including fatty acid biosynthesis, suggesting biotin limitation as a universal factor in bacterial MV formation. Some bacteria are auxotrophic for biotin, including *M. tuberculosis* clinical isolates (Schaefer et al., 1955), and many bacteria that can synthesize

biotin are known to possess transporters to uptake biotin from the environment (Hebbeln et al., 2007), implying that biotin limitation may occur among these bacteria. Furthermore, mammals rely on diet and gut microbes for biotin supply, and it is tempting to speculate that biotin has important roles in host-microbe interaction (Hebbeln et al., 2007; Yoshii et al., 2019), where MVs may also take part. Biotin synthesis has been reported to be essential for *M. tuberculosis* acute infection (Park et al., 2011; Sassetti and Rubin, 2003), and as mammals lack biotin biosynthetic enzymes, biotin biosynthesis is a potential target for antibiotic development (Park et al., 2011), with amiclenomycin and actithiazic acid being examples of such antibiotics that work especially well against mycobacteria (Salaemae et al., 2016). Penicillin G is also reported to be effective for infectious diseases caused by some MCB pathogens including *R. equi* in combination with other antibiotics (Jacks et al., 2003), and our results suggest that antibiotics targeting biotin biosynthesis and cell wall biosynthesis may enhance MV formation, similar to what is observed in other bacteria (Andreoni et al., 2019)(Fulsundar et al., 2014; Manning and Kuehn, 2011).

The involvement of antibiotics in MV formation also has ecological significance as many antibiotics that inhibit DNA replication or the biosynthesis of bacterial cell wall have been found to be produced by bacteria and fungi (Levine, 2006; Umezawa et al., 1966). For example, MMC and penicillin G, which induced MV formation, were originally isolated from *Streptomyces caespitosus* (bacterium) or *Penicillium chrysogenum* (fungus), respectively (Gaynes, 2017; Wakaki et al., 1958). These antibiotic-producing microorganisms are known to exist in complex ecological systems such as soil in which MCB have also been found (Huska and Kaevska, 2012; Komukai-Nakamura et al., 1996; Takai et al., 1991; Udaka, 1960) and may coexist in such environments. Thus, it is possible that MCB experience DNA stress and cell-envelope stress in the environment that generate different types of MVs giving various roles in cell-to-cell interactions (Brown et al., 2015; Domingues and Nielsen, 2017; Kadurugamuwa and Beveridge, 1996; Mashburn and Whitley, 2005; , 2017b; Schwechheimer and Kuehn, 2015).

Our findings would have clinical relevance as some strains of *R. equi* are zoonotic and cause severe pyogranulomatous pneumonia in young horses and immunocompromised humans (Hondalus, 1997). Moreover, *M. smegmatis* is widely used as a non-pathogenic model organism of *M. tuberculosis* and have similar cell envelope structures (Alderwick et al., 2015). Host-induced stresses may ultimately induce MV formation in MCB pathogens, as these pathogens experience DNA damage and attacks of antimicrobial peptides and proteins that cause membrane destabilization during infection (Stallings and Glickman, 2010). A recent study reported that MVs released from *M. avium,* under conditions mimicking the macrophage phagosome, contain dsDNA (Chiplunkar et al., 2019) Notably, it was shown that IMVs released from *M. tuberculosis* are involved in their pathogenesis in mice by modulating immune responses in a TLR2-dependent manner (Prados-Rosales et al., 2011). These observations suggest that IMVs play important roles in the pathogenesis of pathogenic MCB. Our results further show that IMVs are only formed through endolysin-triggered bubbling cell death, and dsDNA is abundant in MVs triggered by bubbling cell death, suggesting that cell wall degradation or alterations are involved in the biogenesis of the MVs observed in the earlier studies. Future work on elucidating each role of different types of MVs may provide us an overall understanding of how MVs are involved in the pathogenicity of MCBs. Finally, as MVs have drawn great attention in application due to its potential as serving as a platform for vaccine development (Acevedo et al., 2014), the basic knowledges in inducing MV formation may facilitate vaccine development against pathogenic MCB based on various types of MVs that are released by the pathogens.

Limitations of study

Although we characterized different MV formation routes in *C. glutamicum*, the biological function of *C. glutamicum* MVs are currently unknown. Accumulating evidences indicate that MVs play roles in immunomodulation and nutrient acquisition in other MCB, but the knowledge about the MV function in these bacteria are limited. Our next challenge would be to unravel the biological function of *C. glutamicum* MVs and how the difference in the formation routes impacts their functions.

In the biochemical analyses for MV composition, we focus on the abundance of the major proteins, which are apparently enriched in certain types of MVs, to clarify the origins of *C. glutamicum* MVs released under different conditions. The abundance of the minor proteins is not described here, and a more intensive proteomics approach may hint the function of the MVs. In addition, there is a potential limitation in our lipid analysis. Although comprehensive lipid analysis clarified mycomembrane- and inner membrane-specific lipids in *C. glutamicum,* which can be used as markers for determining membrane origins of MVs, the

number of these membrane-specific lipids might be underestimated due to limitation in membrane separation selectivity. Finally, we could not determine whether N-MVs formed under normal growing conditions are released from viable cells or dying cells due to fast cell growth and low frequency of MV formation in *C. glutamicum* cells under the tested condition. Considering the biochemical compositions of N-MVs indicating their mycomembrane origin, they are presumably released from viable cells, but this requires further investigation.

Resource availability

Lead contact

Further information and requests for resources and reagents should be directed to and will be fulfilled by the Lead Contact, Masanori Toyofuku (toyofuku.masanori.gf@u.tsukuba.ac.jp).

Materials availability

Plasmids and bacterial strains generated in this study are available from the Lead Contact with a completed Materials Transfer Agreement.

Data and code availability

The datasets supporting the current study are available from the corresponding author on request.

METHODS

All methods can be found in the accompanying Transparent Methods supplemental file.

SUPPLEMENTAL INFORMATION

Supplemental Information can be found online at https://doi.org/10.1016/j.isci.2020.102015.

ACKNOWLEDGMENTS

M.T. and T.N. were supported by Grant-in-aid for Scientific Research from Japanese Society for the Promotion of Science (19H02866 and 19H05682 or 19K15726, respectively). M.M. was supported by Grant-in-aid for Scientific Research (A) from Japanese Society for the Promotion of Science (17H01544) and the Japan Science and Technology Agency (CREST project JPMJCR19S5). N.N. was supported by the Japan Science and Technology Agency (ERATO project JPMJER1502). We appreciate the technical support from Junko Shiomi at Osaka University. We thank the Life Science Center for Survival Dynamics and the Open Facility Network Office, Research Facility Center for Science and Technology, University of Tsukuba, for allowing us to use the UltrafleXtreme-ETA MALDI-TOF/TOF (Bruker), especially Mitsue Arimoto for her great technical assistant and helpful suggestions. We also thank Ajinomoto Co., Inc. for providing the plasmid pVK7. LC/MS analyses were supported by Dr. Koichiro Kako (University of Tsukuba). GC/MS analyses were supported by Dr. Shunsuke Masuo (University of Tsukuba) and Prof. Naoki Takaya (University of Tsukuba). SEM analysis was supported by Dr. Junichi Peter Abe (University of Tsukuba).

AUTHOR CONTRIBUTIONS

T.N. and M.T. designed the research. T.N., Y.O.T., M.M., and M.T. analyzed the data. Y.O.T. conducted the QFDE analysis. T.N. conducted all other experiments. T.N., Y.O.T., M.M., N.N., and M.T. discussed the results. T.N. and M.T. wrote the manuscript.

DECLARATIONS OF INTERESTS

The authors declare no competing interests.

Received: September 8, 2020
Revised: November 20, 2020
Accepted: December 28, 2020
Published: January 14, 2021

REFERENCES

Acevedo, R., Fernández, S., Zayas, C., Acosta, A., Sarmiento, M.E., Ferro, V.A., Rosenqvist, E., Campa, C., Cardoso, D., Garcia, L., and Perez, J.L. (2014). Bacterial outer membrane vesicles and vaccine applications. Front. Immunol. *5*, 121.

Agrawal, A., and Ramachandran, R. (2019). Exploring the links between lipid geometry and mitochondrial fission: Emerging concepts. Mitochondrion *49*, 305–313.

Alderwick, L.J., Harrison, J., Lloyd, G.S., and Birch, H.L. (2015). The mycobacterial cell wall—peptidoglycan and arabinogalactan. Cold Spring Harb. Perspect. Med. *5*, a021113.

Andreoni, F., Toyofuku, M., Menzi, C., Kalawong, R., Shambat, S.M., François, P., Zinkernagel, A.S., and Eberl, L. (2019). Antibiotics stimulate formation of vesicles in *Staphylococcus aureus* in both phage-dependent and -independent fashions and via different routes. Antimicrob. Agents Chemother. *63*, e01439–18.

Arndt, D., Grant, J., Marcu, A., Sajed, T., Pon, A., Liang, Y., and Wishart, D.S. (2016). PHASTER: a better, faster version of the PHAST phage search tool. Nucleic Acids Res. *44*, W16–W21.

Bansal-Mutalik, R., and Nikaido, H. (2011). Quantitative lipid composition of cell envelopes of *Corynebacterium glutamicum* elucidated through reverse micelle extraction. Proc. Natl. Acad. Sci. U S A *108*, 15360–15365.

Beveridge, T.J. (1999). Structures of gram-negative cell walls and their derived membrane vesicles. J. Bacteriol. *181*, 4725–4733.

Brand, S., Niehaus, K., Pühler, A., and Kalinowski, J. (2003). Identification and functional analysis of six mycolyltransferase genes of *Corynebacterium glutamicum* ATCC13032: the genes *cop1*, *cmt1* and *cmt2* can replace each other in the synthesis of trehalose dicorynomycolate, a component of the mycolic acid layer of the cell envelope. Arch. Microbiol. *180*, 33–34.

Brennan, P.J., and Nikaido, H. (1995). The envelope of mycobacteria. Annu. Rev. Biochem. *64*, 29–63.

Brown, L., Wolf, J.M., Prados-Rosales, R., and Casadevall, A. (2015). Through the wall: extracellular vesicles in Gram-positive bacteria, mycobacteria and fungi. Nat. Rev. Microbiol. *13*, 620–630.

Bukovski, A. (2013). Cell envelope of Corynebacteria: structure and influence on pathogenicity. ISRN Microbiol. *2013*, 935736.

Carfrae, L.A., MacNair, C.R., Brown, C.M., Tsai, C.N., Weber, B.S., Zlitni, S., Rao, V.N., Chun, J., Junop, M.S., Coombes, B.K., and Brown, E.D. (2020). Mimicking the human environment in mice reveals that inhibiting biotin biosynthesis is effective against antibiotic-resistant pathogens. Nat. Microbiol. *5*, 93–101.

Chiplunkar, S.S., Silva, C.A., Bermudez, L.E., and Danelishvili, L. (2019). Characterization of membrane vesicles released by *Mycobacterium avium* in response to environment mimicking the macrophage phagosome. Future Mircrobiol. *14*, 293–313.

Difco Laboratories. (1998). Difco Manual, Eleventh Edition (Sparks, MD: Becton Dickinson and Co.).

Domingues, S., and Nielsen, K.M. (2017). Membrane vesicles and horizontal gene transfer in prokaryotes. Curr. Opin. Microbiol. *38*, 16–21.

Dulberger, C.L., Rubin, E.J., and Boutte, C.C. (2020). The mycobacterial cell envelope — a moving target. Nat. Rev. Microbiol. *18*, 47–59.

Fernandes, P., Ferreira, B.S., and Cabral, J.M. (2003). Solvent tolerance in bacteria: role of efflux pumps and cross-resistance with antibiotics. Int. J. Antimicrob. Agents *22*, 211–216.

Frunzke, J., Bramkamp, M., Scweitzer, J.-E., and Bott, M. (2008). Population heterogeneity in *Corynebacterium glutamicum* ATCC13032 caused by prophage CGP3. J. Bacteriol. *190*, 5111–5119.

Fulsundar, S., Harms, K., m Flaten, G.E., Johnsen, P.J., Chopade, B.A., and Nielsen, K.M. (2014). Gene transfer potential of outer membrane vesicles of *Acinetobacter baylyi* and effects of stress on vesiculation. Appl. Environ. Microbiol. *80*, 3469–3483.

Gaynes, R. (2017). The discovery of penicillin-new insights after more than 75 years of clinical use. Emerg. Infect. Dis. *23*, 849–853.

Gujrati, V., Kim, S., Kim, S.H., Min, J.J., Choy, H.E., Kim, S.H., and Jon, S. (2014). Bioengineered bacterial outer membrane vesicles as cell-specific drug-delivery vehicles for cancer therapy. ACS Nano *8*, 1525–1537.

Hashimoto, K., Kawasaki, H., Akazawa, K., Nakamura, J., Asakura, Y., Kudo, T., Shimizu, S., and Nakamatsu, T. (2006). Changes in composition and content of mycolic acids in glutamate-overproducing *Corynebacterium glutamicum*. Biosci. Biotechnol. Biochem. *70*, 22–30.

Hatfull, G.F. (2018). Mycobacteriophages. Microbiol. Spectr. *6*, 10.

Hayashi, A., Mikami, Y., Miyamoto, K., Kamada, N., Sato, T., Mizuno, S., Naganuma, M., Teratani, T., Aoki, R., Fukuda, S., et al. (2017). Intestinal dysbiosis and biotin deprivation induce Alopecia through overgrowth of *Lactobacillus murinus* in mice. Cell Rep. *20*, 1513–1524.

Hebbeln, P., Rodionov, D.A., Alfandega, A., and Eitinger, T. (2007). Biotin uptake in prokaryotes by solute transporters with an optional ATP-binding cassette-containing module. Proc. Natl. Acad. Sci. U S A *104*, 2909–2914.

Hirasawa, T., Saito, M., Yoshikawa, K., Furusawa, C., and Shimizu, H. (2018). Integrated analysis of the transcriptome and metabolome of *Corynebacterium glutamicum* during penicillin-induced glutamic acid production. Biochem. J. *13*, 1700612.

Hoischen, C., and Kräman, R. (1990). Membrane alteration in necessary but not sufficient for effective glutamate secretion in *Corynebacterium glutamicum*. J. Bacteriol. *172*, 3409–3416.

Hondalus, M.K. (1997). Pathogenesis and virulence of *Rhodococcus equi*. Vet. Microbiol. *56*, 257–268.

Huska, K., and Kaevska, M. (2012). Mycobacteria in water, soil, plants and air: a review. Vet. Med-czech *57*, 623–679.

Hünnefeld, M., Persicke, M., Kalinowski, J., and Frunzke, J. (2019). The MarR-type regulator MalR involved in stress-responsive cell envelope remodeling in *Corynebacterium glutamicum*. Front. Microbiol. *10*, 1039.

Jacks, S.S., Giguère, S., and Nguyen, A. (2003). In vitro susceptibilities of *Rhodococcus equi* and other common equine pathogens to azithromycin, clarithromycin, and 20 other antimicrobials. Antimicrob. Agents Chemother. *47*, 1742–1745.

Kadurugamuwa, J.L., and Beveridge, T.J. (1996). Bacteriolytic effect of membrane vesicles from *Pseudomonas aeruginosa* on other bacteria including pathogens: conceptually new antibiotics. J. Bacteriol. *178*, 2767–2774.

Kaparakis-Liaskos, M., and Ferrero, R.L. (2015). Immune modulation by bacterial outer membrane vesicles. Nat. Rev. Immunol. *15*, 375–387.

Kikuchi, Y., Obana, N., Toyofuku, M., Kodera, N., Soma, T., Ando, T., Fukumori, Y., Nomura, N., and Taoka, A. (2020). Diversity of physical properties of bacterial extracellular membrane vesicles revealed through atomic force microscopy phase imaging. Nanoscale *12*, 7950–7959.

Komukai-Nakamura, S., Sugiura, K., Yamauchi-Inomata, Y., Toki, H., Venkateswaran, K., Yamamoto, S., Tanaka, H., and Harayama, S. (1996). Construction of bacterial consortia that degrade arabian light crude oil. J. Ferment. Bioengineer. *82*, 570–574.

Kuru, E., Hughes, H.V., Brown, P.J., Hall, E., Tekkam, S., Cava, F., Pedro, M.A., Brun, Y.V., and VanNieuwenhze, M.S. (2012). *In situ* probing of newly synthesized peptidoglycan in live bacteria with fluorescent D-amino acids. Angew. Chem. Int. Ed. Engl. *51*, 12519–12523.

Kümmerer, K. (2003). Significance of antibiotics in the environment. J. Antimicrob. Chemother. *52*, 5–7.

Larsson, D.G.J. (2014). Antibiotics in the environment. Ups. J. Med. Sci. *119*, 108–112.

Levine, D.P. (2006). Vancomycin: a history. Clin. Infect. Dis. *42*, S5–S12.

Manning, A., and Kuehn, M.J. (2011). Contribution of bacterial outer membrane vesicles to innate bacterial defense. BMC Microbiol. *11*, 258.

Mashburn, L.M., and Whiteley, M. (2005). Membrane vesicles traffic signals and facilitate group activities in a prokaryote. Nature *437*, 422–425.

Matsumoto, K., Kusaka, J., Nishibori, A., and Hara, H. (2006). Lipid domains in bacterial membranes. Mol. Microbiol. *61*, 1110–1117.

Matsuo, H., Chevallier, J., Mayran, N., Blanc, I.L., Ferguson, C., Fauré, J., Blanc, N.S., Matile, S., Dubochet, J., Sadoul, R., et al. (2004). Role of LBPA and Alix in multivesicular liposome formation and endosome organization. Science *303*, 531–534.

Mileykovskaya, E., and Dowhan, W. (2000). Visualization of phospholipid domains in *Escherichia coli* by using the cardiolipin-specific fluorescent dye 10-*N*-nonyl acridine orange. J. Bacteriol. *182*, 1172–1175.

Mileykovskaya, E., and Dowhan, W. (2009). Cardiolipin membrane domains in prokaryotes and eukaryotes. Biochem. Biophys. Acta *1788*, 2084–2091.

Nagakubo, T., Nomura, N., and Toyofuku, M. (2020). Cracking open bacterial membrane vesicles. Front. Microbiol. *10*, 3026.

Nakamura, J., Hirano, S., Ito, H., and Wachi, M. (2007). Mutations of the *Corynebacterium glutamicum* NCgl1221 gene, encoding a mechanosensitive channel homolog, induce L-glutamic acid production. Appl. Environ. Microbiol. *73*, 4491–4498.

Nakayama, Y., Hashimoto, K., Sawada, Y., Sokabe, M., Kawasaki, H., and Martinac, B. (2018). *Corynebacterium glutamicum* mechanosensitive channels: towards unpuzzling "glutamate efflux" for amino acid production. Biophys. Rev. *10*, 1359–1369.

Nanda, A.M., Heyer, A., Krämer, C., Grünberger, A., Kohlheyer, D., and Frunzke, J. (2014). Analysis of SOS-induced spontaneous prophage induction in *Corynebacterium glutamicum* at the single-cell level. J. Bacteriol. *196*, 180–188.

Nara, T., Samejima, H., and Kinoshita, S. (1964). Effect of penicillin on amino acid fermentation. Agric. Biol. Chem. *28*, 120–124.

Ochiai, K., Takayama, K., and Kawamoto, I. (1987). Cytological changes in *Corynebacterium glutamicum* cell envelope structure caused by biotin deficiency. Actinomycetologica *1*, 31–42.

Park, S.W., Klotzsche, M., Wilson, D.J., Boshoff, H.I., Eoh, H., Manjunatha, U., Blumenthal, A., Rhee, K., Barry, C.E., III, Aldrich, C.C., et al. (2011). Evaluating the sensitivity of *Mycobacterium tuberculosis* to biotin deprivation using regulated gene expression. PLoS Pathog. *7*, e1002264.

Portevin, D., Sousa-D'Auria, C.D., Houssin, C., Grimaldi, C., Chami, M., Daffé, M., and Guilhot, C. (2004). A polyketide synthase catalyzes the last condensation step of mycolic acid biosynthesis in mycobacteria and related organisms. Proc. Natl. Acad. Sci. U S A *101*, 314–319.

Prados-Rosales, R., Baena, A., Martinez, L.R., Luque-Garcia, J., Kalscheuer, R., Veeraraghavan, U., Camara, C., Nosanchuk, J.D., Bersa, G.S., Chen, B., et al. (2011). Mycobacteria release active membrane vesicles that modulate immune responses in a TLR2-dependent manner in mice. J. Clin. Invest. *121*, 1471–1483.

Prados-Rosales, R., Weinrick, B.C., Daniel, G.P., Jacobs, W.R., Casadevall, A., and Rodriguez, G.M. (2014). Role for *Mycobacterium tuberculosis* membrane vesicles in iron acquisition. J. Bacteriol. *196*, 1250–1256.

Puech, V., Bayan, N., Salim, K., Leblon, G., and Daffé, M. (2000). Characterization of the *in vivo* acceptors of the mycoloyl residues transferred by the corynebacterial PS1 and the related mycobacterial antigens 85. Mol. Microbiol. *35*, 1026–1041.

Raad, R.B., Méniche, X., Sousa-d'Auria, C., Chami, M., Salmeron, C., Tropis, M., Daffé, M., Houssin, C., and Bayan, N. (2010). A deficiency in arabinogalactan biosynthesis affects *Corynebacterium glutamicum* mycolate outer membrane stability. J. Bacteriol. *192*, 2691–2700.

Renner, L.D., and Weibel, D.B. (2011). Cardiolipin microdomains localize to negatively curved regions of *Escherichia coli* membranes. Proc. Natl. Acad. Sci. U S A *108*, 6264–6269.

Robbins, P.D., and Morelli, A.E. (2014). Regulation of immune responses by extracellular vesicles. Nat. Rev. Immunol. *14*, 195–208.

Roier, S., Zingl, F.G., Caker, F., Durakovic, S., Kohl, P., Eichmann, T.O., Klug, L., Gadermaier, B., Weinzerl, K., Prassl, R., et al. (2016). A novel mechanism for the biogenesis of outer membrane vesicles in Gram-negative bacteria. Nat. Commun. *7*, 10515.

Salaemae, W., Booker, G.W., and Polyak, S.W. (2016). The role of biotin in bacterial physiology and virulence: a novel antibiotic target for *Mycobacterium Tuberculosis*. Microbiol. Spectr. *4*, 2.

Sandmann, G., and Yukawa, H. (2005). Vitamin synthesis: carotenoids, biotin and pantothenate (Chapter 17). In Handbook of Corynebacterium Glutamicum, L. Eggeling and M. Bott, eds. (CRC press), pp. 359–383.

Sassetti, C.M., and Rubin, E.J. (2003). Genetic requirements for mycobacterial survival during infection. Proc. Natl. Sci. Acad. U S A *28*, 12989–12994.

Schaefer, W.B., Cohn, M.L., and Middlebrook, G. (1955). The roles of biotin and carbon dioxide in the cultivation of *Mycobacterium tuberculosis*. J. Bacteriol. *69*, 706–712.

Schwechheimer, C., and Kuehn, M.J. (2015). Outer-membrane vesicles from Gram-negative bacteria: biogenesis and functions. Nat. Rev. Microbiol. *13*, 605–619.

Shiio, I., Otsuka, S.I., and Takahashi, M. (1962). Effect of biotin on the bacterial formation of glutamic acid. I. Glutamate formation and cellular permeability of amino acids. J. Biochem. *51*, 56–62.

Smith, I. (2003). *Mycobacterium tuberculosis* pathogenesis and molecular determinants of virulence. Clin. Microbiol. Rev. *16*, 463–496.

Stallings, C.L., and Glickman, M.S. (2010). Is *Mycobacterium tuberculosis* stressed out? A critical assessment of the genetic evidence. Microbes Infect. *12*, 14–15.

Sutterlin, H.A., Shi, H., May, K.L., Miguel, A., Khare, S., Huang, K.C., and Silhavy, T.J. (2016). Disruption of lipid homeostasis in the Gram-negative cell envelope activates a novel cell death pathway. Proc. Natl. Acad. Sci. U S A *113*, E1565–E1574.

Takai, S., Ohbushi, S., Koike, K., Tsubaki, S., Oishi, H., and Kamada, M. (1991). Prevalence of virulent *Rhodococcus equi* in isolates from soil and feces of Horces from Horce-Breeding Farms with and without endemic infections. J. Clin. Microbiol. *29*, 2887–2889.

Theresia, N.M., Aida, K., Takada, A., Iwai, N., and Wachi, M. (2018). Effects of EGTA on cell surface structures of *Corynebacterium glutamicum*. Arch. Microbiol. *200*, 281–289.

Toledo, A., Huang, Z., Coleman, J.L., London, E., and Benach, J.L. (2018). Lipidrafts can form in the inner and outer membranes of *Borrelia burgdorferi* and have different properties and associated proteins. Mol. Microbiol. *108*, 63–76.

Toyofuku, M., Cárcamo-Oyarce, G., Yamamoto, T., Eisenstein, F., Hsiao, C.C., Kurosawa, M., Gademann, K., Pilhofer, M., Nomura, N., and Eberl, L. (2017a). Prophage-triggered membrane vesicle formation through peptidoglycan damage in *Bacillus subtilis*. Nat. Commun. *8*, 481.

Toyofuku, M., Morinaga, K., Hashimoto, Y., Uhl, J., Shimamura, H., Inaba, H., Schmitt-Kopplin, P., Eberl, L., and Nomura, N. (2017b). Membrane vesicle-mediated bacterial communication. ISME J. *11*, 1504–1509.

Toyofuku, M., Nomura, N., and Eberl, L. (2019). Types and origins of bacterial membrane vesicles. Nat. Rev. Microbiol. *17*, 13–24.

Trajkovic, K., Hsu, C., Chiantia, S., Rajendran, L., Wenzel, D., Wieland, F., Schwille, P., Brügger, B., and Simons, M. (2008). Ceramide triggers budding of exosome vesicles into multivesicular endosomes. Science *319*, 1244–1247.

Tulum, I., Tahara, Y.O., and Miyata, M. (2019). Peptidoglycan layer and disruption processes in *Bacillus subtilis* cells visualized using quick-freeze, deep-etch electron microscopy. Microscopy *68*, 441–449.

Turnbull, L., Toyofuku, M., Hynen, A.L., Kurosawa, M., Pessi, G., Petty, N.K., Osvath, S.R., Cárcamo-Oyarce, G., Gloag, E.S., Shimoni, R., et al. (2016). Explosive cell lysis as a mechanism for the biogenesis of bacterial membrane vesicles and biofilms. Nat. Commun. *14*, 11220.

Udaka, S. (1960). Screening method for microorganisms accumulating metabolites and its use in isolation of *Micrococcus glutamicus*. J. Bacteriol. *79*, 754–755.

Umezawa, H., Maeda, K., Takeuchi, T., and Okami, Y. (1966). New antibiotics, bleomycin A and B. J. Antibiot. *19*, 200–209.

Vidakovics, M.L., Jendholm, J., Mörgelin, M.A., Larsson, C., Cardell, L.O., and Riesbeck, K. (2010). B cell activation by outer membrane vesicles—a novel virulence mechanism. PLoS Pathog. *6*, e1000724.

Wakaki, S., Marumo, H., Tomioka, K., Shimizu, G., Kato, E., Kamada, H., Kudo, S., and Fujimoto, Y. (1958). Isolation of new fractions of antitumor mitomycins. Antibiot. Chemother. *8*, 228–240.

Wang, M., Nie, Y., and Wu, X.L. (2020). Extracellular heme recycling and sharing across species by novel mycomembrane vesicles of a Gram-positive bacterium. ISME J. https://doi.org/10.1038/s41396-020-00800-1.

Wang, X., Thompson, C.D., Weidenmaier, C., and Lee, J.C. (2018). Release of *Streptococcus aureus* extracellular vesicles and their application as a vaccine platform. Nat. Commun. *9*, 1379.

Wollert, T., and Hurley, J.H. (2010). Molecular mechanism of multivesicular body biogenesis by ESCRT complexes. Nature *464*, 864–869.

Yang, J., and Yang, S. (2017). Comparative analysis of *Corynebacterium glutamicum* genomes: a new perspective for the industrial production of amino acids. BMC Genomics *18*, 940.

Yoshii, K., Hosomi, K., Sawane, K., and Kunisawa, J. (2019). Metabolism of dietary and microbial vitamin B family in the regulation of host immunity. Front. Nutr. *6*, 48.

Zingl, F.G., Kohl, P., Caker, F., Leitner, D.R., Mitterer, F., Bonnington, K.E., Rechberger, G.N., Kuehn, M.J., Guan, Z., Riedl, J., and Schild, S. (2019). Outer membrane vesiculation facilitates surface exchange and *in vivo* adaptation of *Vibrio cholerae*. Cell Host Microbe *27*, 225–237.

Zuber, B., Chami, M., Houssin, C., Dubochet, J., Griffiths, G., and Daffé, M. (2008). Direct visualization of the outer membrane of mycobacteria and corynebacteria in their native state. J. Bacteriol. *190*, 5672–5680.

iScience, Volume *24*

Supplemental Information

Mycolic acid-containing bacteria trigger distinct types of membrane vesicles through different routes

Toshiki Nagakubo, Yuhei O. Tahara, Makoto Miyata, Nobuhiko Nomura, and Masanori Toyofuku

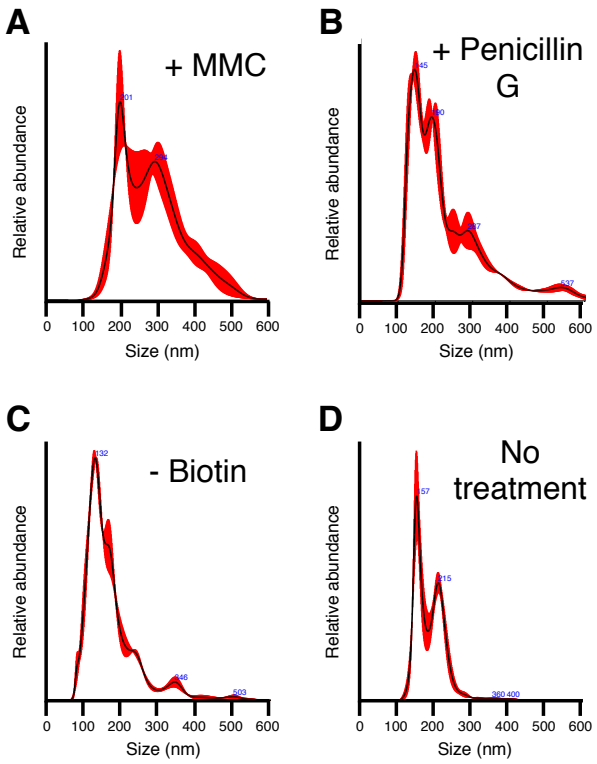

Supplemental Figure 1. Size distributions of MVs. Related to Fig. 1.

Particle size distributions of (A) M-MVs, (B) P-MVs, (C) B-MVs and (D) N-MVs. Black lines indicate the mean values of the relative concentrations of the detected particles for three experiments. Red regions indicate ± S. D. of the mean values.

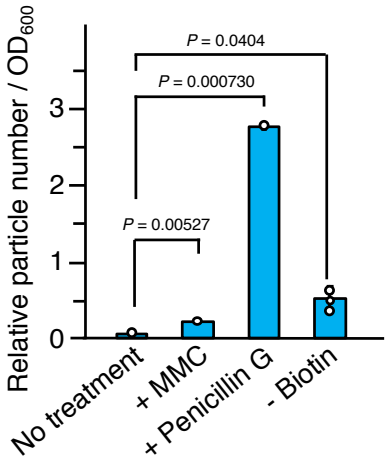

Supplemental Figure 2. Relative concentrations of *Corynebacterium glutamicum* MVs. Related to Fig. 1.

C. glutamicum MVs were analysed by nanoparticle tracking using Nanosight and the calculated particle concentrations were normalised to OD_{600}. *P* values were calculated using unpaired *t*-test with Welch's correction. All values indicated by the bars are the mean ± S. D. for three experiments.

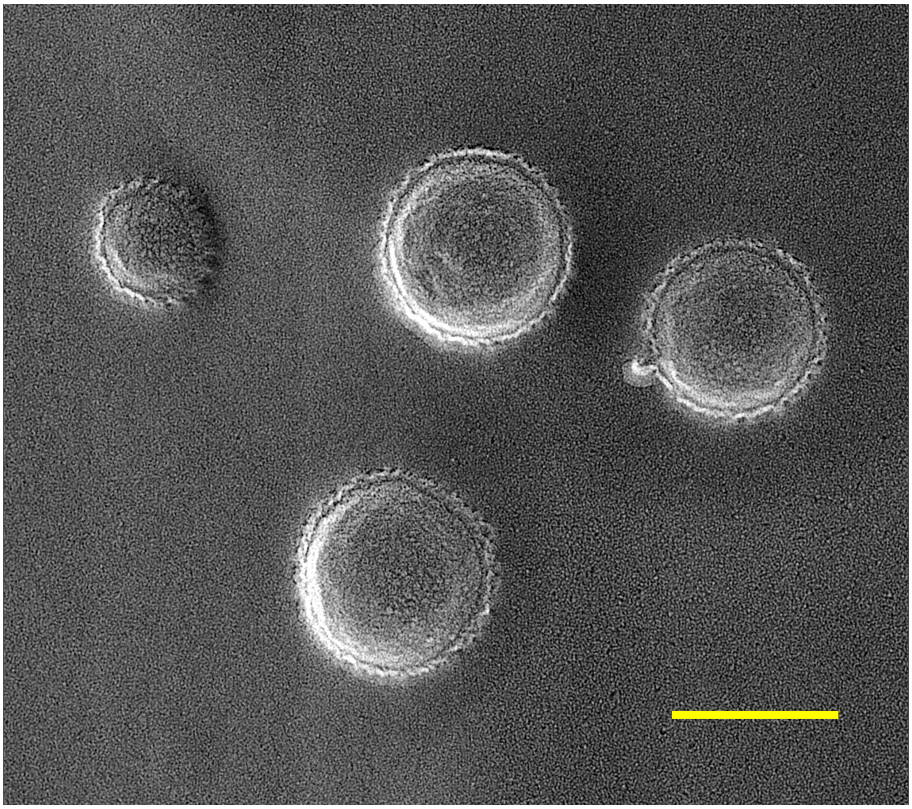

Supplemental Figure 3. QFDE image of N-MVs. Related to Fig. 1.

QFDE image of N-MVs shows lipid bilayer structures. Scale bar, 200 nm. The image shows MVs whose outer leaflet of the lipid bilayer was stripped off, exposing the inner leaflet of the lipid bilayer. The outer leaflet of the lipid bilayer was stripped off due to the tendency of the fracture plane to follow a plane through the hydrophobic core of the membrane at cryogenic temperature. Glycerol was added before cryo fixation.

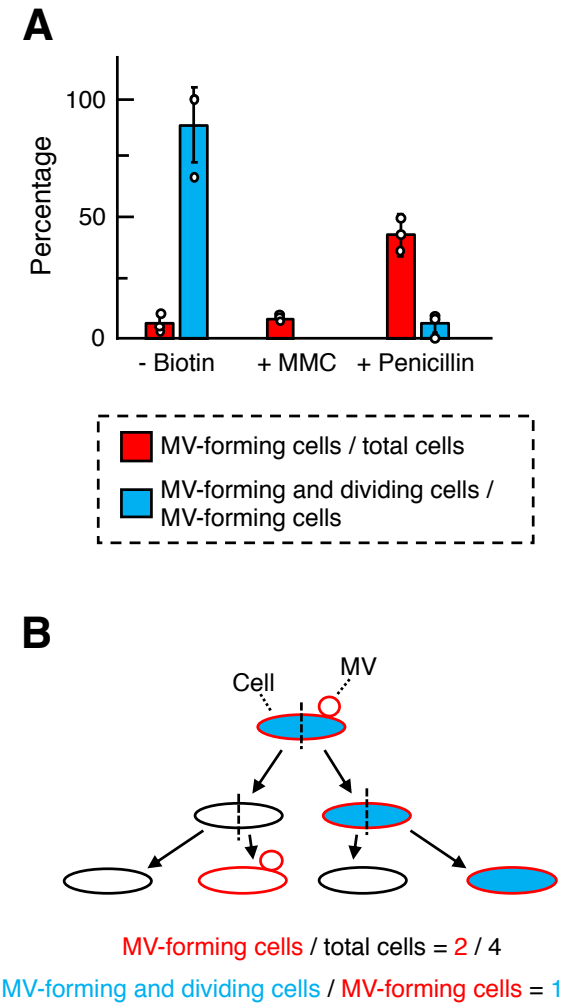

Supplemental Figure 4. Populations of MV-forming cells. Related to Fig. 2.

Populations of MV-forming cells were counted during time-lapse imaging using CLSM. (A) Percentages of MV-forming cells per total cells (red bars) and MV-forming and growing cells per total MV-forming cells (blue bars) were calculated. Cells that divided during the observation for ~5 hours were defined as dividing cells. All values indicated by the bars represent the mean value ± S.D. for 3 fields. In total, 208, 413, and 206 cells were counted in biotin deficiency, under MMC and penicillin G conditions, respectively. (B) Schematic diagram of a method for counting MV-forming cells in this study.

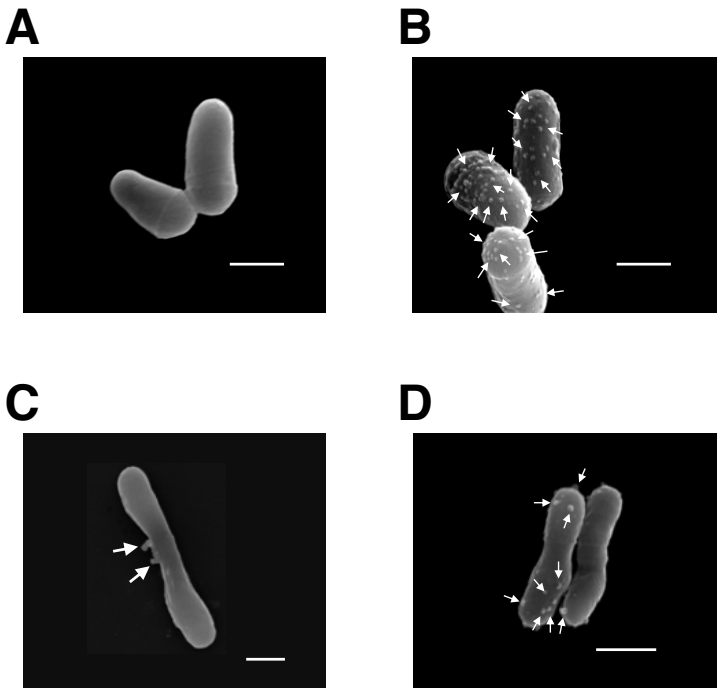

Supplemental Figure 5. Scanning electron microscopy images of *Corynebacterium glutamicum* cells. Related to Fig. 1 and Fig. 2.

C. glutamicum cells under (A) no treatment, (B) biotin-deficient, (C) MMC treatment, and (D) penicillin G treatment conditions were fixed and observed by scanning electron microscopy. White arrows indicate MVs. Scale bars, 1 μm.

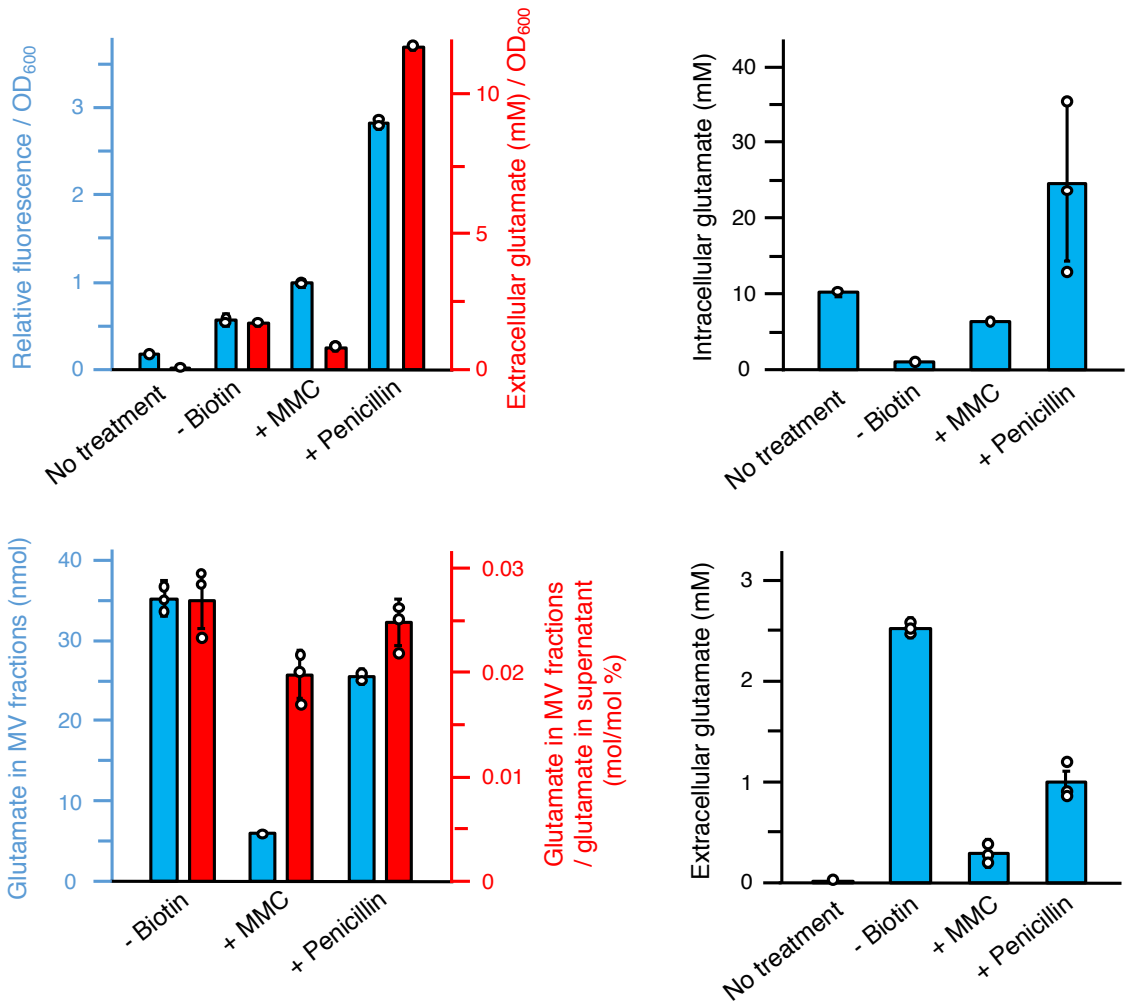

Supplemental Figure 6. Glutamate effluxes of *Corynebacterium glutamicum* under various conditions. Related to Fig. 1 and Fig. 2.

(A) Concentrations of glutamate in the culture media of *C. glutamicum*. (B) MV release (blue) and the concentrations of glutamate in the culture media (red) were normalised to OD_{600}. (C) Intracellular glutamate concentrations of *C. glutamicum* cells that were grown under MV release-inducing conditions. These concentrations were calculated using dried cell weight of the cells. (D) Glutamate was detected and quantified from MVs. Percentages are glutamate in MV fractions to total glutamate in culture supernatant before MV isolation. MVs were purified from 200 mL of the culture medium, and then glutamate was extracted from these MVs (blue). These values were compared with the total amounts of glutamate in the culture supernatant (red). All values indicated by the bars represent the mean value ± S.D. for three experiments.

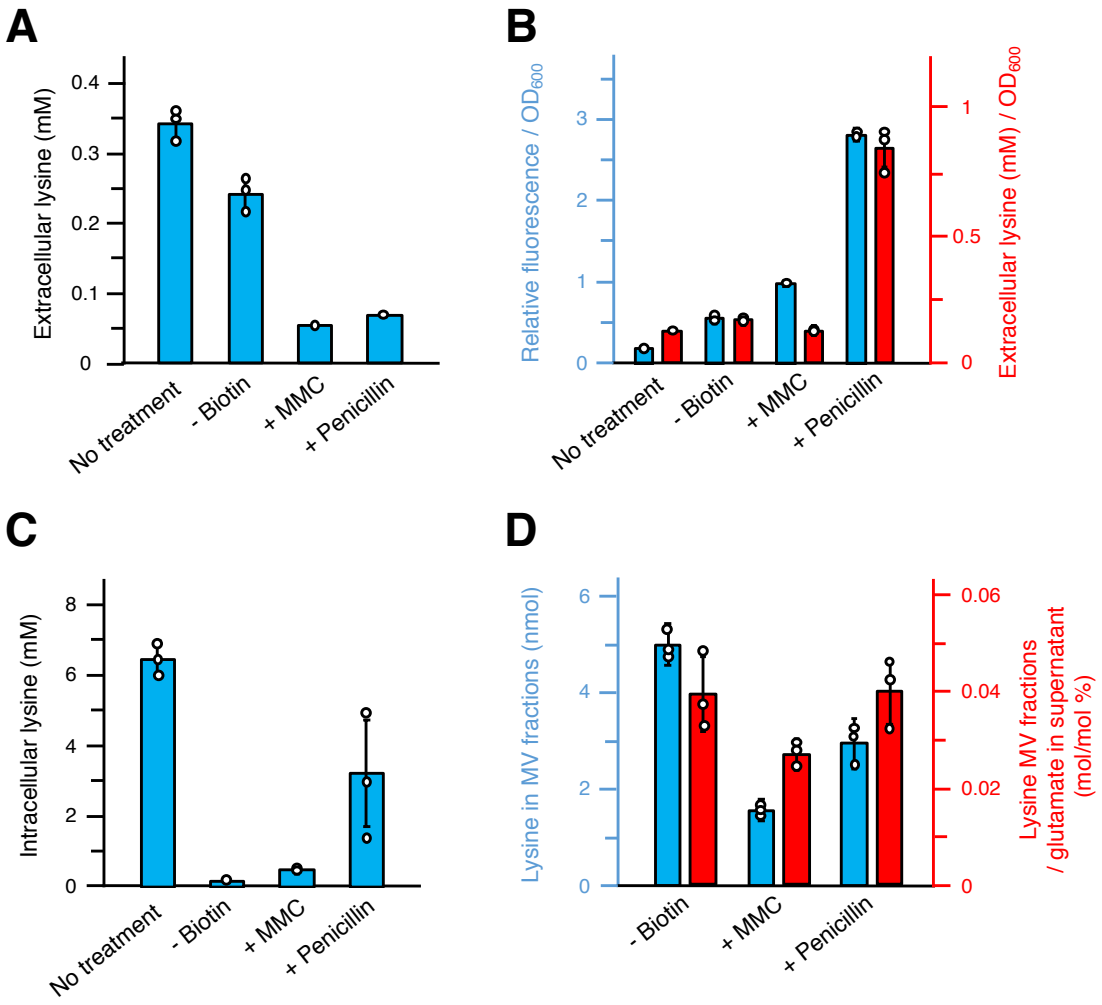

Supplemental Figure 7. Lysine effluxes of *Corynebacterium glutamicum* under various conditions. Related to Fig. 1 and Fig. 2.

(A) Concentrations of lysine in the culture media of *C. glutamicum*. (B) MV release (blue) and the concentrations of lysine in the culture media (red) were normalised to OD_{600}. (C) Concentrations of intracellular lysine of *C. glutamicum* cells that were grown under MV release-inducing conditions. These concentrations were calculated using dried cell weight of the cells. (D) Lysine was detected and quantified from MVs. Percentages are lysine in MV fractions to total lysine in culture supernatant before MV isolation. MVs were purified from 200 mL of the culture medium, and then lysine was extracted from these MVs (blue). These values were compared with the total amounts of lysine in the culture supernatant (red). All values indicated by the bars represent the mean value ± S.D. for three experiments.

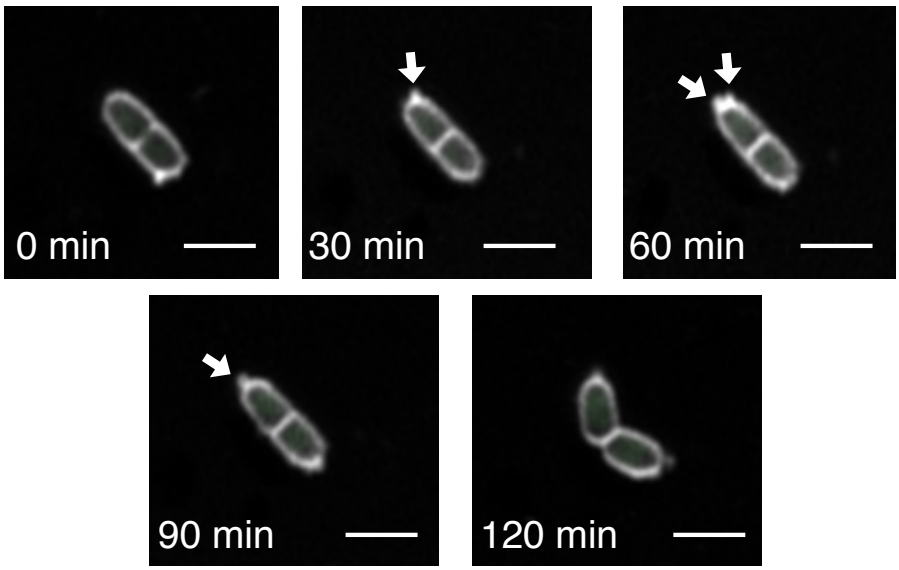

Supplemental Figure 8. Cell division after MV formation in penicillin G condition. Related to Fig. 2.

Cell division of *Corynebacterium glutamicum* cell after MV formation was observed during time-lapse imaging using CLSM in the presence of penicillin G. White arrows indicate MVs. Representative images are shown. White, FM4-64; green, SYTOX green. Scale bar, 2 μm.

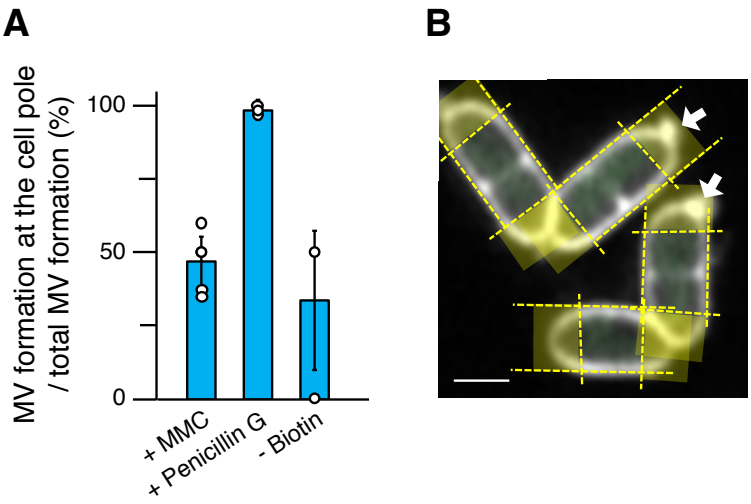

Supplemental Figure 9. MV formation at the cell pole in *Corynebacterium glutamicum*. Related to Fig. 2.

(A) MV formation at the cell pole in *C. glutamicum* was counted using live-cell imaging. *C. glutamicum* was cultured on agarose pad containing MM-1 medium under MMC treatment, penicillin G treatment or biotin-deficient condition. The cells were observed using CLSM for ~5 hours. All values indicated by the bars represent the mean value ± S.D. for 5 fields. (B) A representative image of the cells under penicillin G treatment condition is shown. Curved regions at the end of the rod-shaped cells (yellow regions) were defined as the cell poles under all conditions. White arrows indicate MVs. Scale bar, 1 μm.

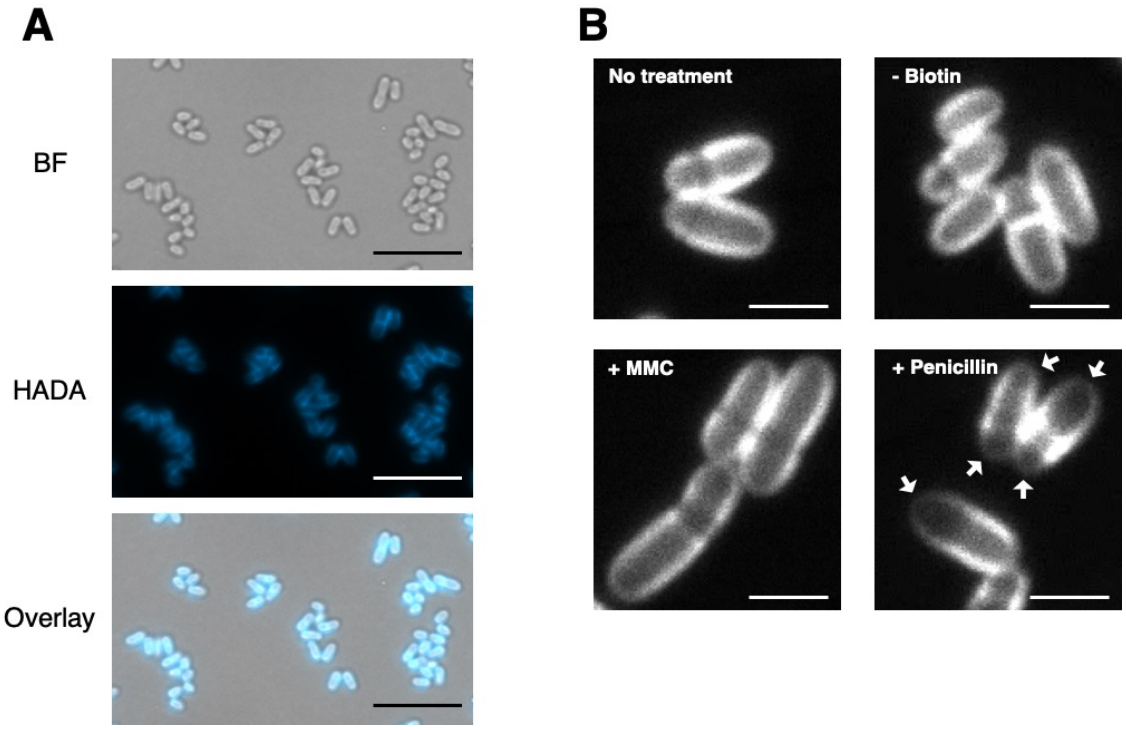

Supplemental Figure 10. Peptidoglycan staining using HADA. Related to Fig. 2.

Peptidoglycans of *Corynebacterium glutamicum* cells were stained by adding HADA to the culture medium. (A) Bright field (BF, top), fluorescence microscopy (middle) and overlay (bottom) of HADA-stained cells under no treatment condition. Scale bars, 10 μm. (B) CLSM images of HADA-stained cells under no treatment or MV formation-inducing conditions. White arrows indicate cell poles where peptidoglycan biosynthesis was inhibited. The images of the cells under normal condition (No treatment) and under penicillin G condition (+Penicillin) were also shown in Fig. 2. Scale bars, 2 μm.

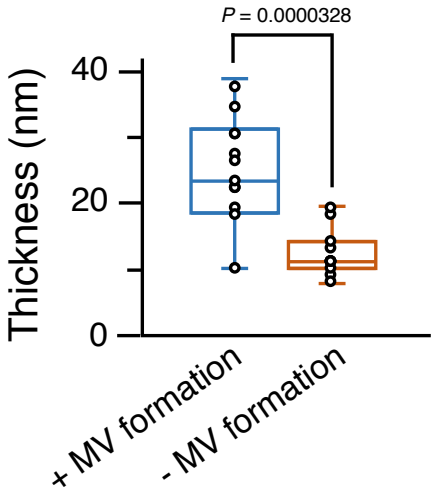

Supplemental Figure 11. MV formation outside of electron-transparent layers of *Corynebacterium glutamicum* cells in biotin deficiency. Related to Fig. 2.

Box plot of thickness of electron-transparent layers (ETLs) in the cell envelope of *C. glutamicum* cells in biotin deficiency. The blue box (left) indicates maximum thickness of the ETLs where MV formations were observed in TEM images of the cells in biotin deficient condition. The orange box (right) indicates thickness of randomly selected ETLs where no MV formation was observed in the same condition. Sample numbers, 14 each. *P* value was calculated using unpaired *t*-test with Welch's correction.

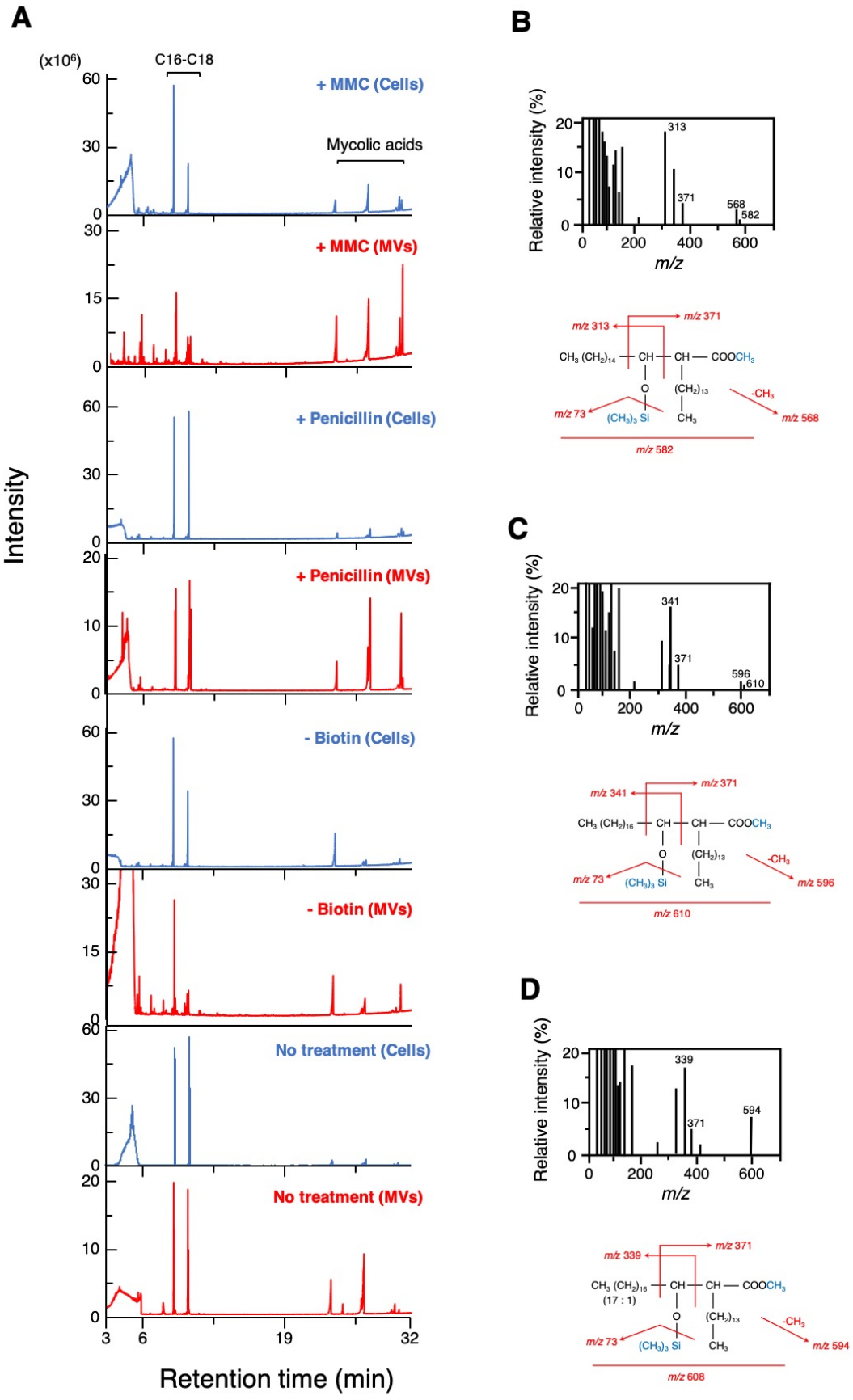
A
(x10⁶)
C16-C18
Mycolic acids
+ MMC (Cells)
+ MMC (MVs)
+ Penicillin (Cells)
+ Penicillin (MVs)
- Biotin (Cells)
- Biotin (MVs)
No treatment (Cells)
No treatment (MVs)
Intensity
Retention time (min)
B
Relative intensity (%)
m/z
313
371
568
582
m/z 313
m/z 371
m/z 73
m/z 568
m/z 582
C
Relative intensity (%)
m/z
341
371
596
610
m/z 341
m/z 371
m/z 73
m/z 596
m/z 610
D
Relative intensity (%)
m/z
339
371
594
m/z 339
m/z 371
m/z 73
m/z 594
m/z 608

Supplemental Figure 12. Structures of corynomycolic acids that were detected in *Corynebacterium glutamicum* cells and MVs. Related to Fig. 3.

(A) Detection of fatty acids by gas chromatography/mass spectrometry (GC/MS). The lipids were extracted from lyophilised cells and MVs. C16-C18 fatty acids and C32-C34 corynomycolic acids were detected as methylester and methylester-trimethylsilyl derivatives, respectively. (B-D) The structures of corynomycolic acids were determined based on the fragmentation patterns on GC/MS analyses and a previous study (Hashimoto et al, 2006).

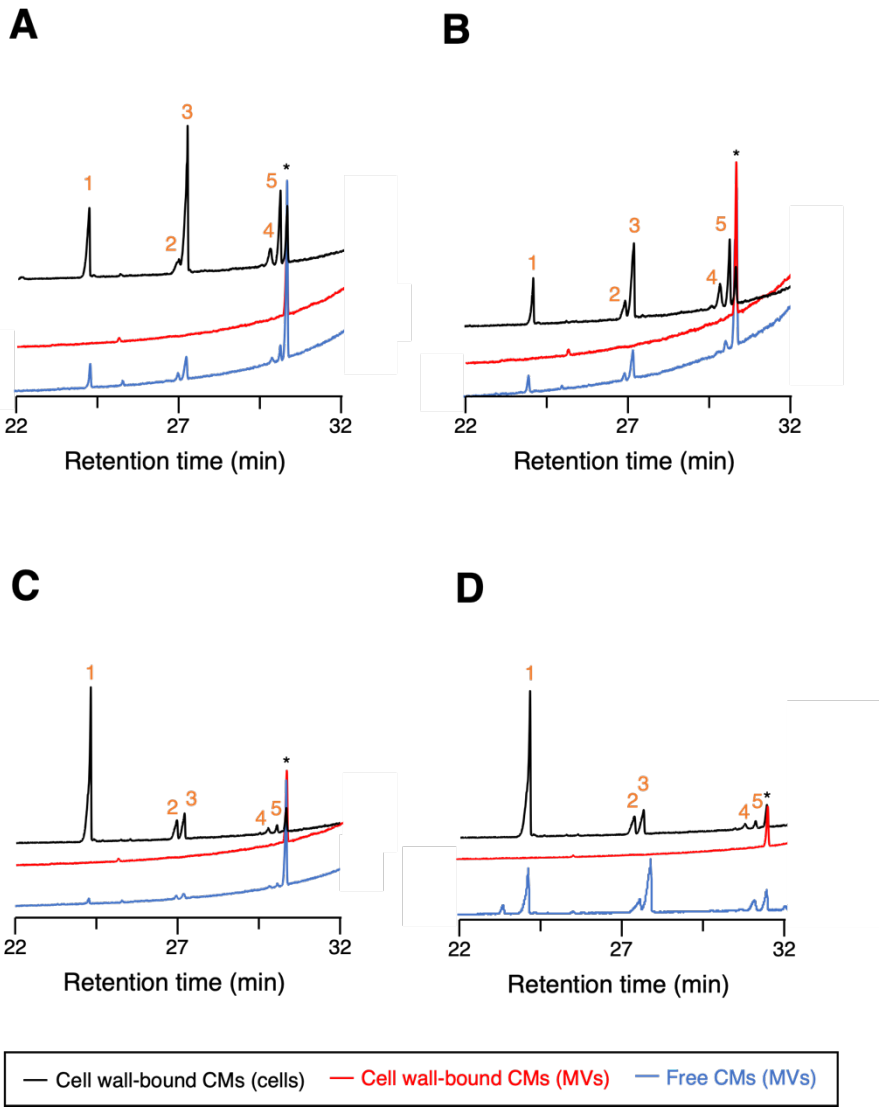

Supplemental Figure 13. GC/MS analyses of corynomycolic acids that are free or covalently bound to cell wall. Related to Fig. 3.

Corynomycolic acids (CMs) were extracted from cell walls and analysed by GC/MS. Cell wall-bound CMs were extracted and derivatised by hydrolysis of corynomycolic acids (CM)-arabinogalactan-peptidoglycan complex from the cells and MVs. Free CMs were sequentially extracted from MVs using MeOH: $CHCl_3$ = 2:1, 1:1 and 1:2 solutions. Cells were grown under (A) MMC treatment, (B) penicillin treatment and (C) biotin-deficient and (D) no treatment conditions, and the corresponding MVs were purified. Each number indicates the following CMs: 1, C32 CM (*m/z* 582); 2, C34:1 CM (*m/z* 608); 3, C34 CM (*m/z* 610); 4 and 5, undetermined CMs that exhibit *m/z* values of 638 and 636, respectively. The structures of these CMs were determined in Supplemental Fig. 12. Asterisk, solvent-derived peaks.

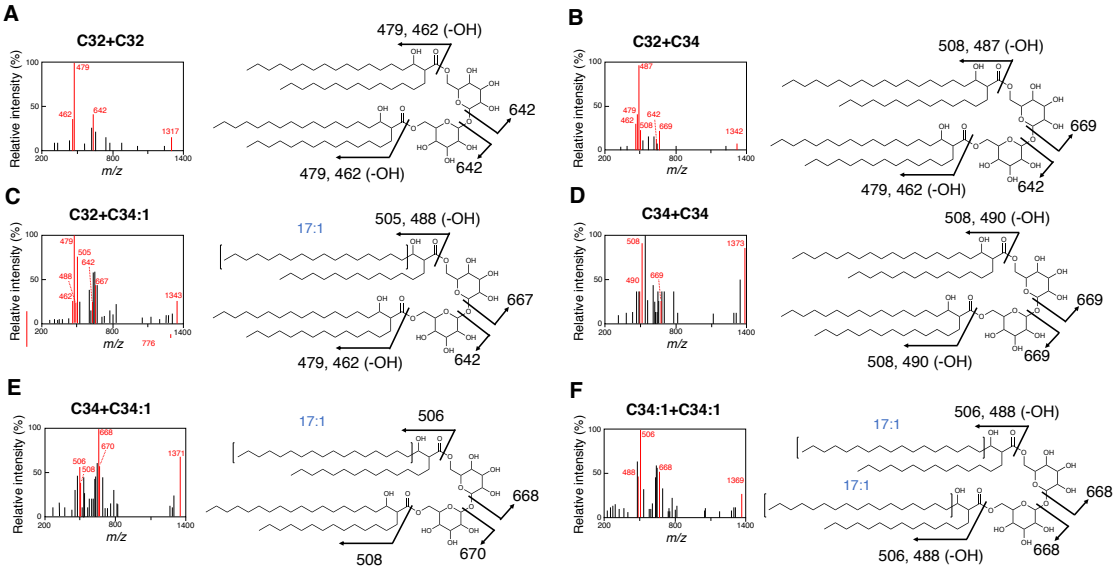

Supplemental Figure 14. Detection of trehalose dicorynomycolic acids from MVs. Related to Fig. 3.

Trehalose dicorynomycolic acids (a-f, TDCMs) were detected from MVs using LC/MS/MS. Representative results are shown. These molecules were searched from the lipid extracts of MVs based on the results of GC/MS analyses.

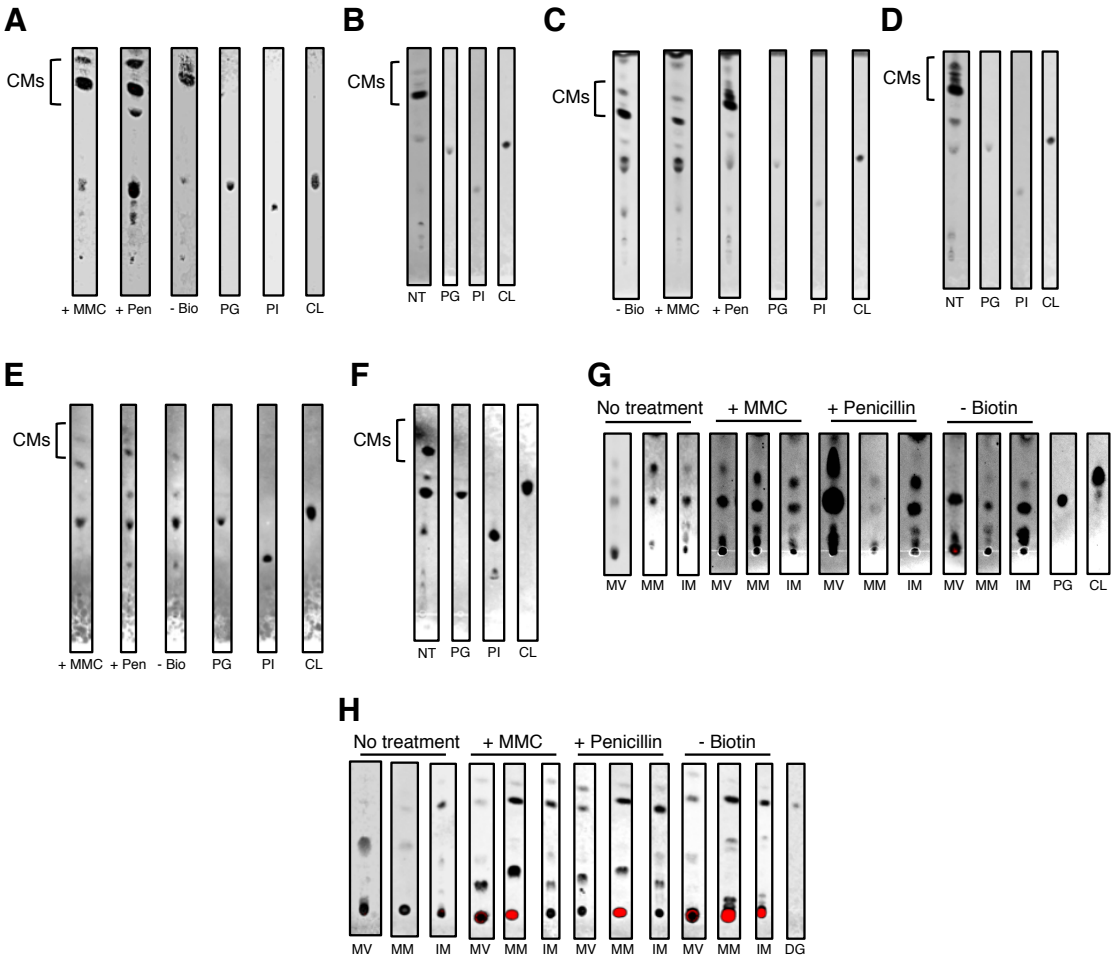

Supplemental Figure 15. Thin-layer chromatography profiles of *Corynebacterium glutamicum* cells and MVs. Related to Fig. 3.

Major lipids in cells and MVs were detected by thin-layer chromatography (TLC). Phosphatidylglycerols (PGs), phosphatidylinositols (PIs), cardiolipins (CLs) and corynomycolic acids (CMs) in (A, B) MVs fractions, (C, D) cellular mycomembrane fractions and (E, F) cellular inner membrane fractions were separated using chloroform:methanol:H_2O = 65:25:4 (v/v) as a solvent. NT, no treatment condition; +MMC, MMC treatment condition; +Pen, penicillin G treatment condition; -Bio, biotin-deficient condition. (G) PG and CL were separated using chloroform: hexane: methanol: acetate = 50:30:10:5 (v/v) as a solvent. (H) Diacylglycerols (DG) were separated using toluene: chloroform: acetone = 7:2:1 (v/v) as a solvent. L-α-phosphatidyl-DL-glycerol (distearoyl), phophatidylinositol, cardiolipin from bovine heart and 1,2-dipalmitoyl-*rac*-glycerol were used as standards. All lipids were labelled with primuline and detected at 365 nm.

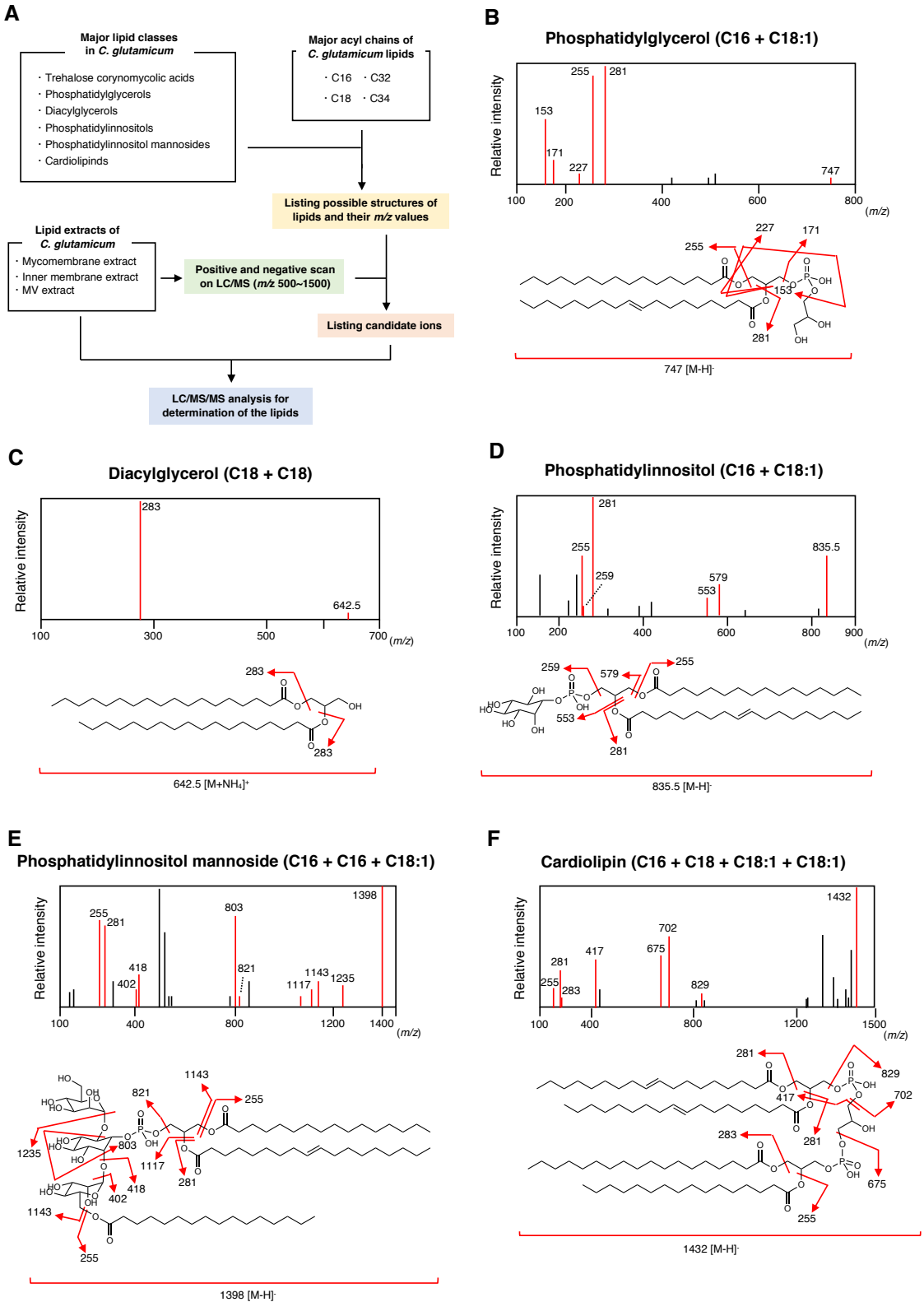
A
Major lipid classes in C. glutamicum
· Trehalose corynomycolic acids
· Phosphatidylglycerols
· Diacylglycerols
· Phosphatidylinnositols
· Phosphatidylinnositol mannosides
· Cardiolipinds
Major acyl chains of C. glutamicum lipids
· C16 · C32
· C18 · C34
Listing possible structures of lipids and their m/z values
Lipid extracts of C. glutamicum
· Mycomembrane extract
· Inner membrane extract
· MV extract
Positive and negative scan on LC/MS (m/z 500~1500)
Listing candidate ions
LC/MS/MS analysis for determination of the lipids
B
Phosphatidylglycerol (C16 + C18:1)
Relative intensity
(m/z)
747 [M-H]-
C
Diacylglycerol (C18 + C18)
642.5 [M+NH4]+
D
Phosphatidylinnositol (C16 + C18:1)
835.5 [M-H]-
E
Phosphatidylinnositol mannoside (C16 + C16 + C18:1)
1398 [M-H]-
F
Cardiolipin (C16 + C18 + C18:1 + C18:1)
1432 [M-H]-

Supplemental Figure 16. Identification of major lipids in *Corynebacterium glutamicum*. Related to Fig. 3.

Lipids of *C. glutamicum* were detected and determined. Schematic diagram of the determination of the lipids is shown in *A*. Major classes of the lipids in *C. glutamicum* are determined based on previous studies (Brennan et al, 1995; Klatt et al, 2018) and our thin-layer chromatography analyses (Supplemental Fig. 15). Based on our results of GC/MS analysis indicating that acyl chain lengths of major lipids in *C. glutamicum* under the tested condition were C16, C18, C32 and C34 (Supplemental Fig. 12), we listed the possible structures of the major lipids which include these fatty acids. We then analysed the lipid extracts of *C. glutamicum* (described under Methods) on LC/MS in the scanning mode. In this analysis, we searched ions whose *m/z* values correspond to those of the listed lipids and then listed these ions as candidate ions derived from *C. glutamicum* lipids. Structures of the candidate ions were determined by LC/MS/MS analysis. (B-F) Representative results of LC/MS/MS analysis of the lipids are shown. Structures of the lipids containing C16 and/or C18 fatty acids were determined based on *m/z* values of their fragment ions and the fragmentation patterns. The fragmentation patterns and the determined structures are consistent with those of previous studies (Cox et al, 2009; Hsu et al, 2001, 2007; Kind et al, 2013; Minkler et al, 2010; Mishra et al, 2009). Characteristics of each class of lipids in the LC/MS/MS analysis are as follows. Phosphatidylglycerol (B) is characterised by $[M-H]^-$ precursor ion and the fragment ions derived from fatty acid chains and phosphate. Diacylglycerol (C) is characterised by $[M+NH_4]^+$ precursor ion and the fragment ions derived from fatty acid chains. Phosphatidylinnositol (D) is characterised by $[M-H]^-$ precursor ion and the fragment ions derived from fatty acid chains and inositol phosphate. Phosphatidylinnositol mannoside (E) is characterised by $[M-H]^-$ precursor ion, the fragment ions derived from fatty acid chains and innositol phosphate, and neutral loss of a mannoside moiety. Cardiolipin (F) is characterised by $[M-H]^-$ precursor ion and the fragment ions derived from fatty acid chains and two phosphatidylglycerol moiety. Details of the analyses are described under Methods. Determined structures of trehalose dicorynomycolic acids containing C32 and/or C34 acyl chains are shown in Supplemental Fig. 14.

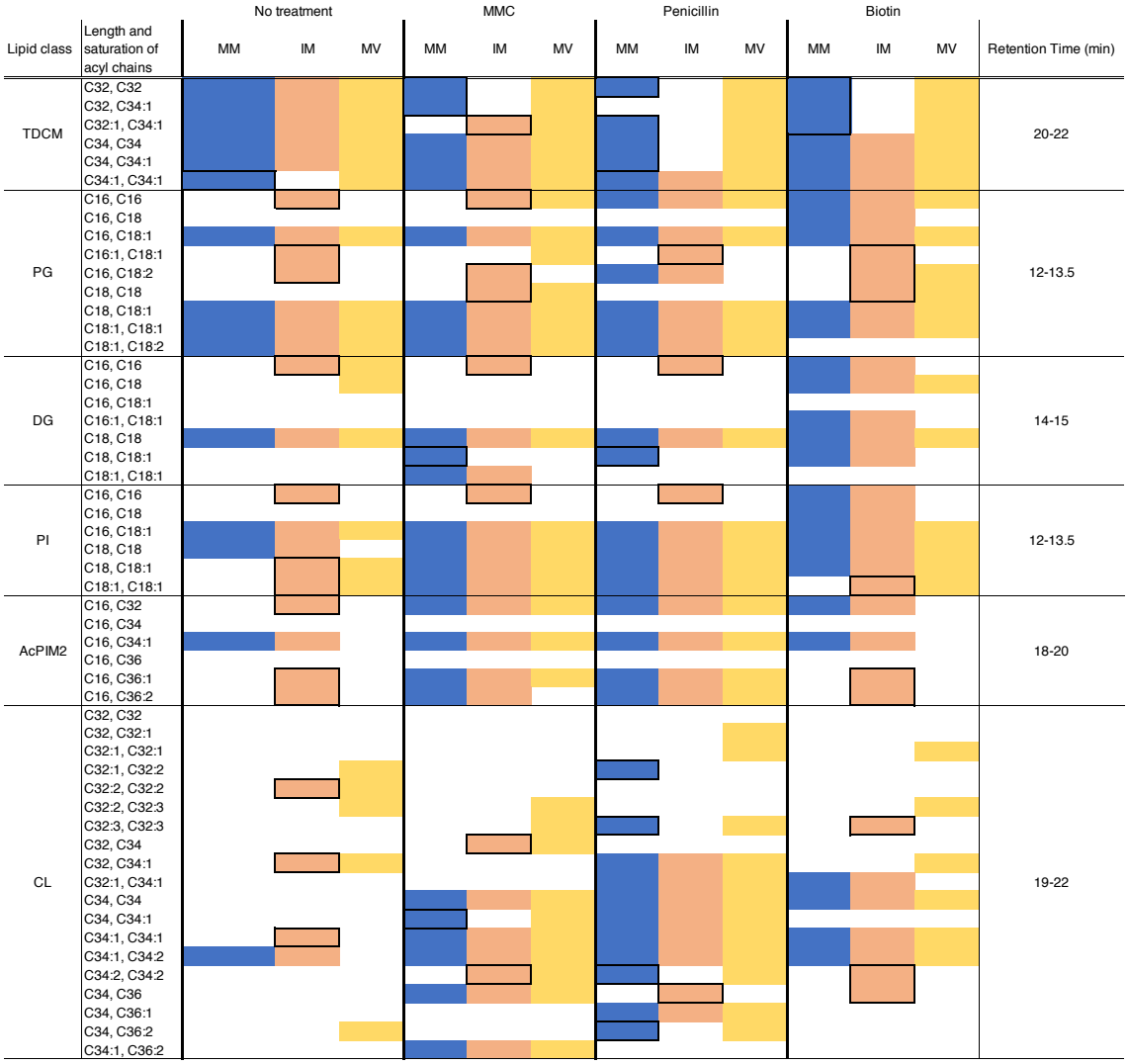

Supplemental Figure 17. Catalogue of the membrane lipids of *Corynebacterium glutamicum*. Related to Fig. 3.

Major lipids in *C. glutamicum* were analysed and listed. Detail of the analysis is described under Methods and Supplemental Fig. 16. The detected lipids are indicated as blue (mycomembrane, MM), orange (inner membrane, IM) or yellow (MV fraction). The lipids that were detected exclusively in mycomembrane or inner membrane are indicated by black bold squares. TDCM, trehalose dicorynomycolic acid; PG, phosphatidylglycerol; DG, diacylglycerol; PI, phosphatidylinnositol; AcPIM2, acylated phosphatidylinnositol mannoside; CL, cardiolipin.

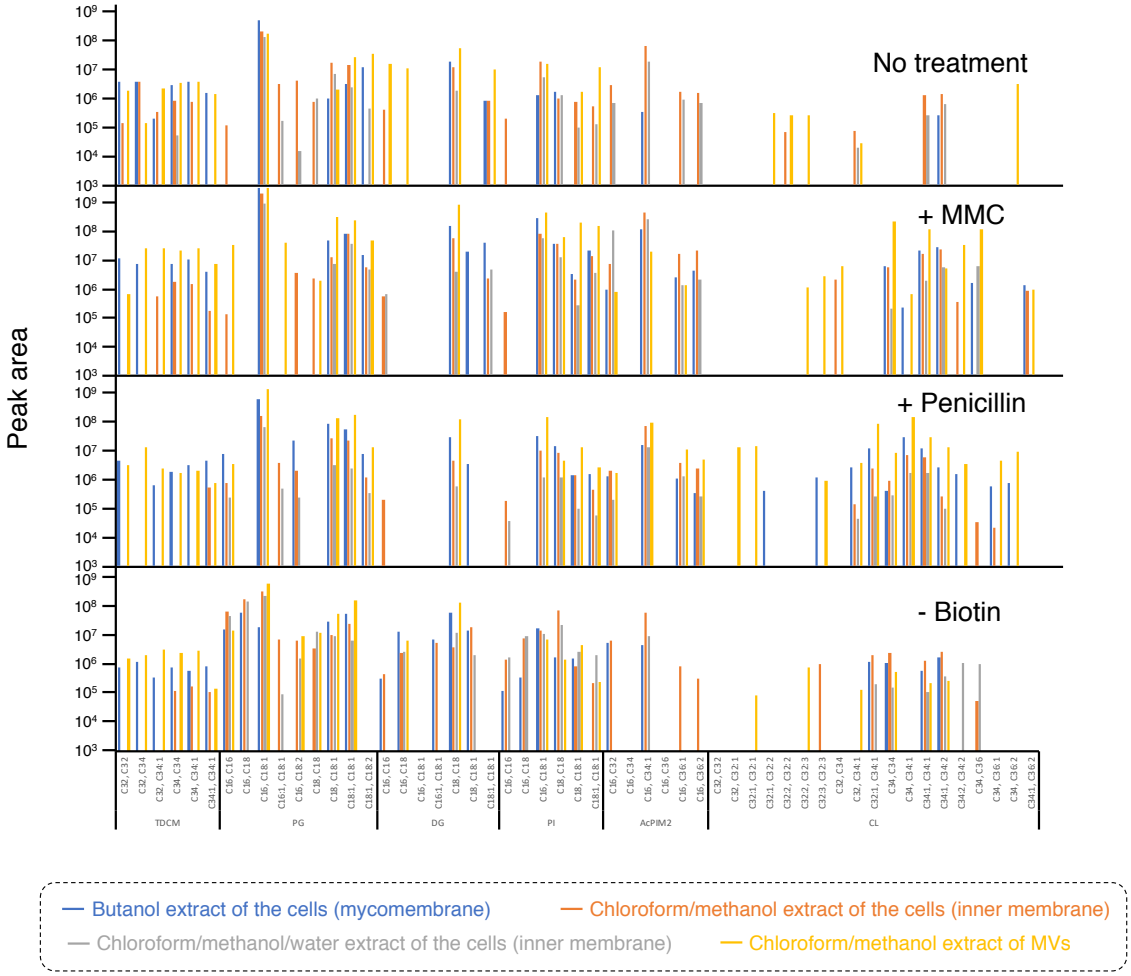

Supplemental Figure 18. Intensities of the membrane lipids of *Corynebacterium glutamicum* in LC/MS analysis. Related to Fig. 3.

Lipid compositions of MVs were analysed by LC/MS. Detail of the analysis is described under Methods. Major lipids in *Corynebacterium glutamicum* were detected and identified based on fragmentation patterns of the lipids on LC/MS/MS analysis (Supplemental Fig. 16) and the previous studies (Cox et al, 2009; Hsu et al, 2001, 2007; Kind et al, 2013; Minkler et al, 2010; Mishra et al, 2009). Average values of three independent experiments are shown. PG, phosphatidylglycerol; DG, diacylglycerol; PI, phosphatidylinositol; AcPIM2, acyl phosphatidyl-*myo*-inositol dimannnoside; CL, cardiolipin.

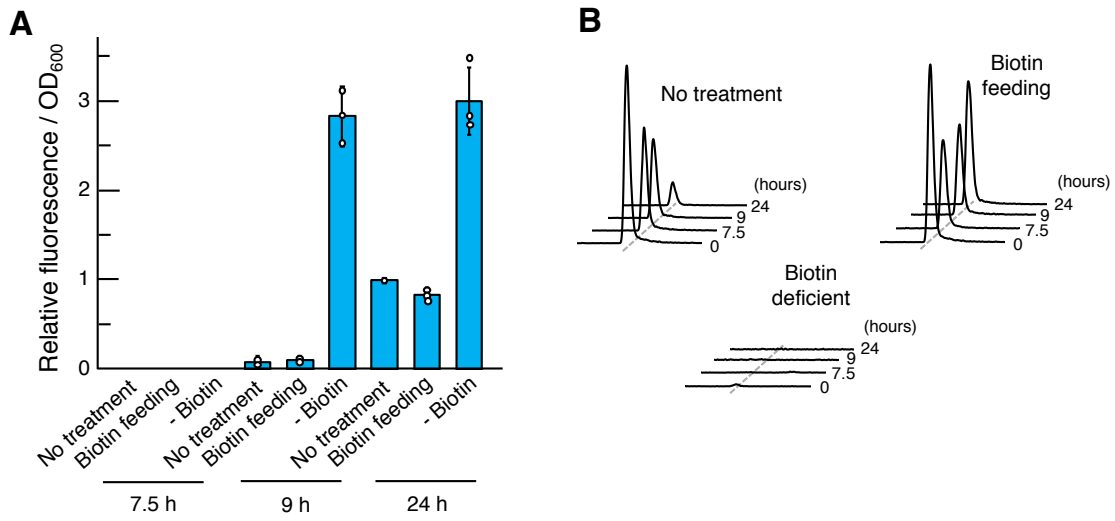

Supplemental Figure 19. *Corynebacterium glutamicum* releases MVs even under biotin-sufficient condition. Related to Fig. 3.

(A) MVs were isolated and quantified from the culture media at each time point during cultivation. No treatment and biotin-deficient (-Biotin) conditions contain 200 and 1 μg L^{-1} biotin, respectively. In biotin-feeding condition, biotin (200 μg L^{-1}) was added to the culture medium of no treatment condition after 9 h of cultivation. All values indicated by the bars represent the mean value ± S.D. for three experiments. (B) Biotin was detected from each culture medium by LC/MS as a product ion which exhibits *m/z* value of 227 in the positive ion mode. Representative chromatograms were shown.

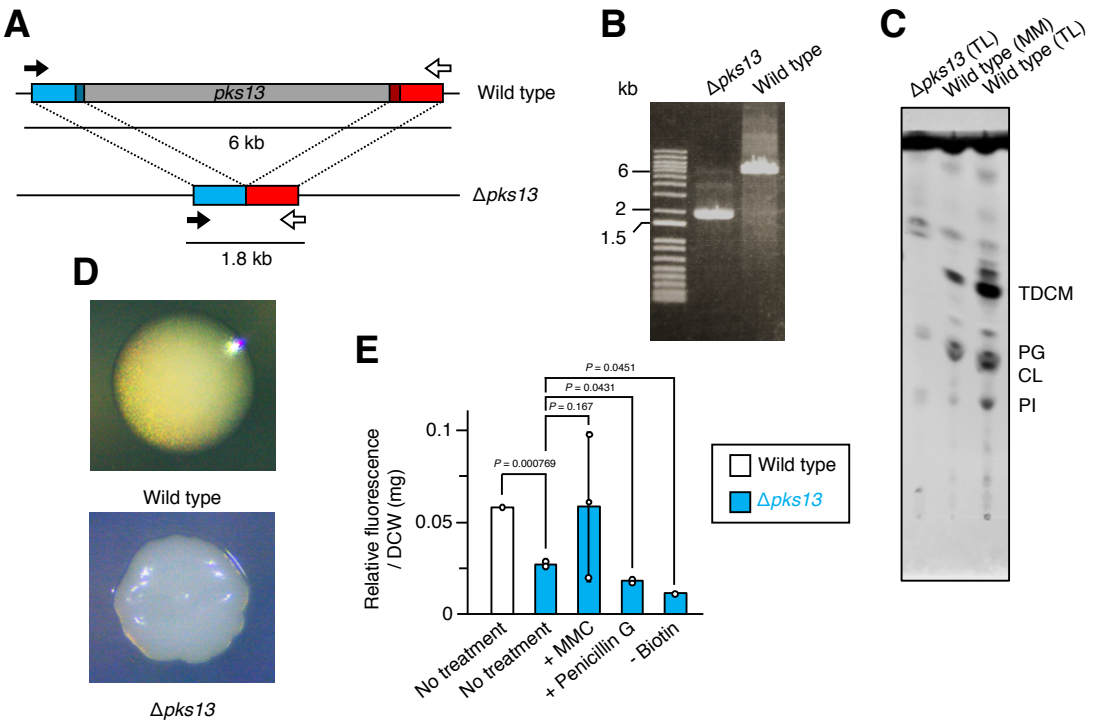

Supplemental Figure 20. MV release by Δ*pks13* mutant of *Corynebacterium glutamicum*. Related to Fig. 3.

(A) Schematic diagram of deletion of *pks13* gene coding a polyketide synthase (PKS13) which catalyzes the last condensation step in the biosynthesis of CMs (Portevin et al, 2004). Arrows indicate the primer set (PKS13_Check_Fw and PKS13_Check_Rv) used for PCR in *B.* (C) TLC analysis of the lipids from wild type and Δ*pks13* mutant of *C. glutamicum*. The lipids were separated using chloroform: methanol: H_2O = 65:25:4 (v/v) as a solvent. TL, total lipids; MM, mycomembrane. (D) Colony morphology of wild type and Δ*pks13* mutant of *C. glutamicum*. (E) MV release of wild type and Δ*pks13* mutant of *C. glutamicum*. Growth conditions were described under Methods. MVs were quantified using FM4-64 dye, and the relative fluorescence were normalised to dried cell weight (DCW). All values indicated by the bars represent the mean value ± S.D. for three experiments. *P*-values were calculated using *t*-test with Welch's correction.

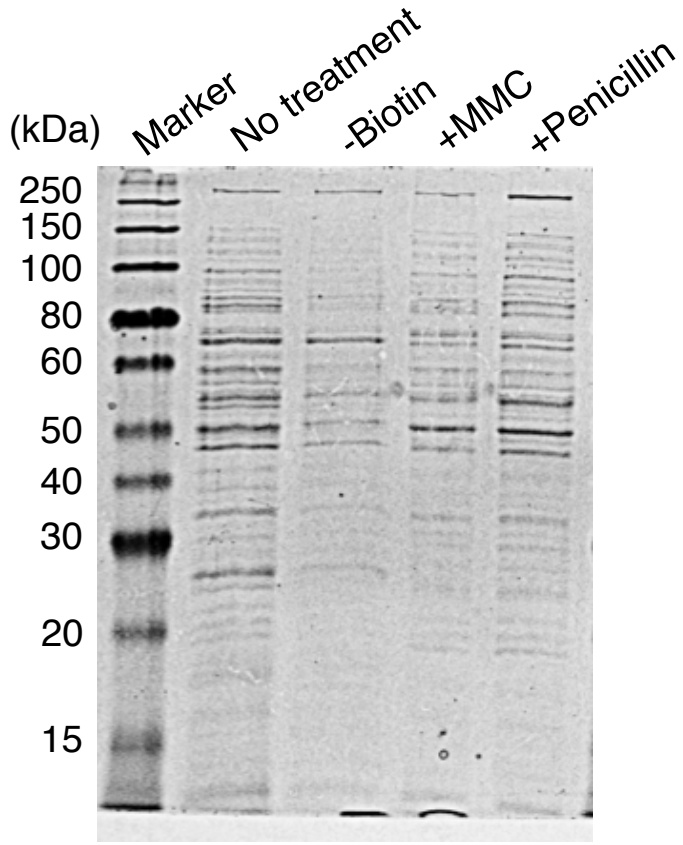

Supplemental Figure 21. SDS-PAGE of *Corynebacterium glutamicum*-derived proteins. Related to Fig. 4.

SDS-PAGE profiles of whole-cell proteins of *C. glutamicum* are shown. After cultivation of *C. glutamicum* in biotin deficiency and under MMC or penicillin G conditions, whole-cell proteins were obtained from the cells by sonication, and subjected to SDS-PAGE. Five micrograms of proteins were applied to each lane.

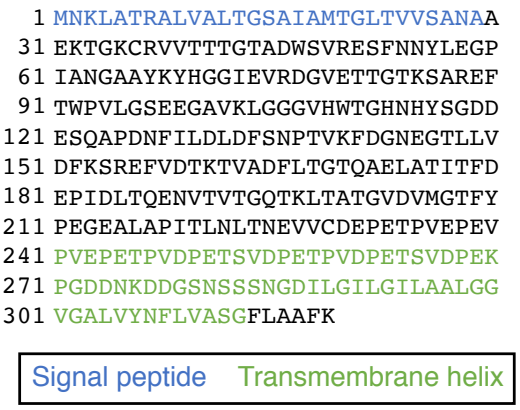

Supplemental Figure 22. Amino acid sequence of NCgl0381. Related to Fig. 4.

Amino acid sequence of NCgl0381 was analysed using SignalP 5.0 (Armenteros et al, 2019) and SOSUI (Mitaku et al, 2002). Blue and green regions indicate the deduced signal peptide and transmembrane helix, respectively, in NCgl0381.

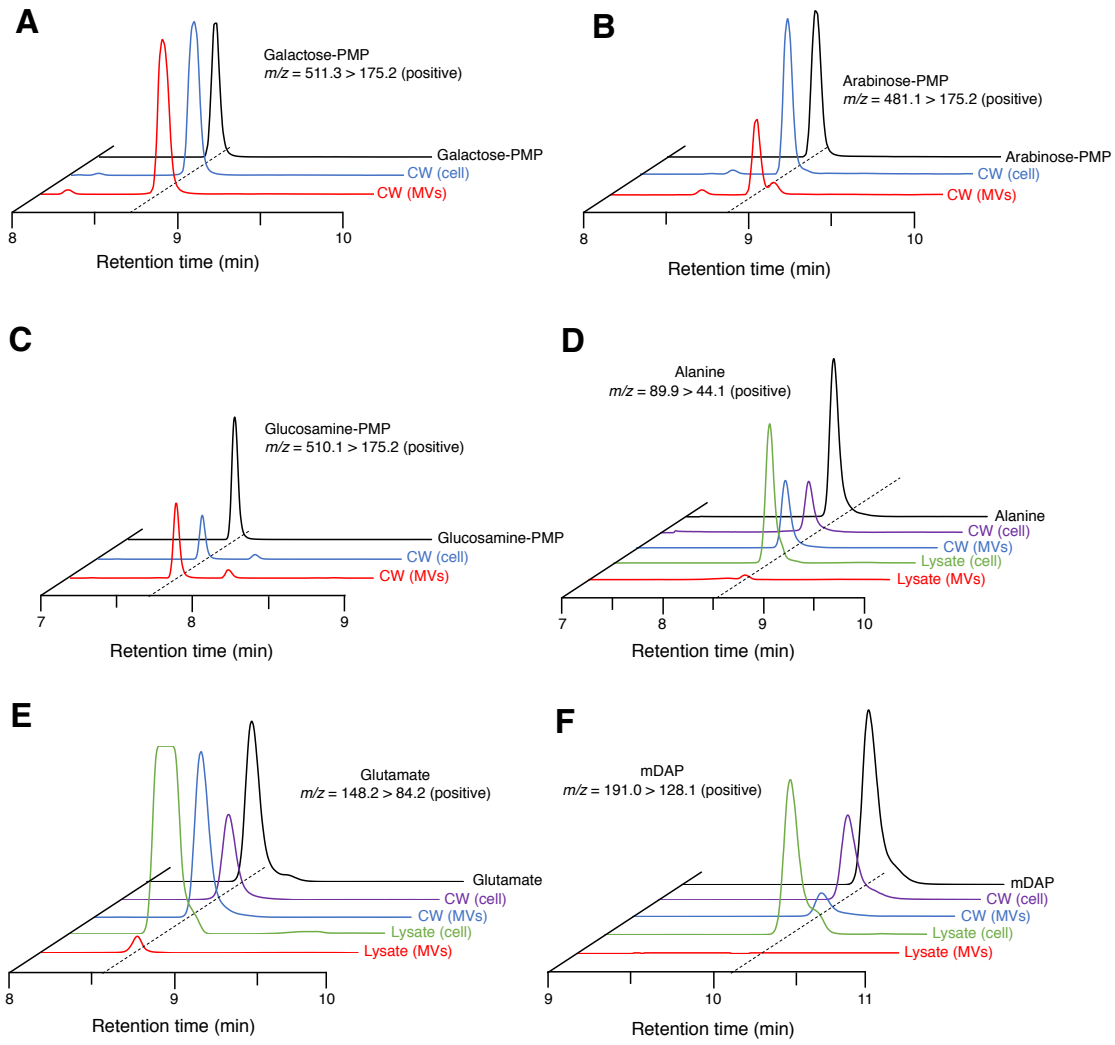

Supplemental Figure 23. Detection of cell wall components from M-MVs. Related to Fig. 4.

Cell wall fragments (CW) were purified from M-MVs and then hydrolysed. (A, B) Arabinogalactan and (C-F) peptidoglycan components were detected by multiple reaction monitoring (MRM) mode using LC/MS. Sugars were derivatised with 3-methyl-1-phenyl-5-pyrazolone (PMP) and then subjected to the analyses.

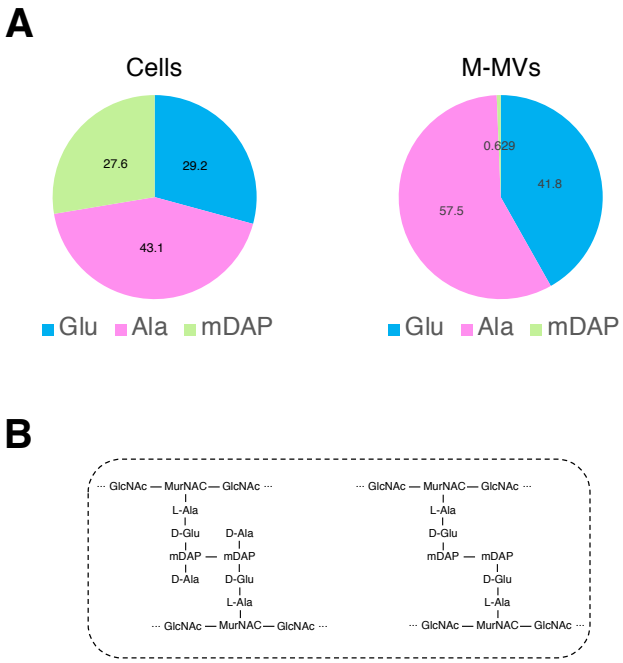

Supplemental Figure 24. Compositions of amino acids of peptidoglycan in *Corynebacterium glutamicum* cells and M-MVs. Related to Fig. 4.

(A) Molar ratio of amino acids of purified peptidoglycan were calculated based on the results of LC/MS analyses. The peptidoglycan was purified from MMC-treated cells and M-MVs. (B) Two types of peptide bridges are present in the peptidoglycan of *C. glutamicum* (Bukovski, 2013).

Supplemental Table 1. Bacterial strains used in this study. Related to Fig. 1 to Fig. 5.

Bacterial strains used in this study and their characteristics are shown.

Strains	Characteristics
Corynebacterium glutamicum ATCC13032 (NBRC12168)	Wild-type strain
Corynebacterium glutamicum Δ*NCgl1682*	Δ*NCgl1682* mutant of wild-type strain
Corynebacterium glutamicum Δ*pks13*	Δ*pks13* mutant of wild-type strain
Mycobacterium smegmatis MC^2155	Wild-type strain
Rhodococcus erythropolis PR4	Wild-type strain
Rhodococcus equi IFO3730	Wild-type strain
Escherichia coli DH5α	F^-, Φ80d*lacZ*ΔM15, Δ(*lacZYA-argF*)U169, *deoR*, *recA*1, *endA*1, *hsdR*17(r_K^-, m_K^+), *phoA*, *supE*44, λ^-, *thi*1, *gyrA*96, *relA*1

Supplemental Table 2. Primers and plasmids used in this study. Related to Fig. 1 to Fig. 3.

(A) Names and nucleotide sequences of primers used in this study are shown. Cleavage sites for restriction enzymes are underlined. (B) Names and characteristics of plasmids used in this study are shown.

A

Primers	Sequences
NCgl1682_FR1_Fw (EcoRI)	TATGACCATGATTACGAATTTCCCTCTAAACAAAACCACCAATTC
NCgl1682_FR1_Rv	AAGGTAAAGGACAAACGAACTGTAGTGGTAGAGGGTTAAAAAAAC
NCgl1682_FR2_Fw	GTTCGTTTGTCCTTTACCTTTAC
NCgl1682_FR2_Rv (HindIII)	ACGACGGCCAGTGCCAAGCTTCAATGGAGAATTTTGGACC
NCgl1682_Ex_Fw (PstI)	CCAAGCTTGCATGCCGAACTGGGTGTAGTGATTTCTGTT
NCgl1682_Ex_Rv (BamHI)	GAGCTCGGTACCCGGGGATCAAAAAACAGCCATCAACATAACGTT
PKS13_FR1_Fw (EcoRI)	TATGACCATGATTACGAATTTCACAGGTGCATACACTGCG
PKS13_FR1_RV	GAATGCTGTCCATGATGACCGA
PKS13_FR2_Fw	GGTCATCATGGACAGCATTCGGAGGTGTCCAGCAGGTTTTC
PKS13_FR2_Rv (HindIII)	ACGACGGCCAGTGCCAAGCTCGACGATGCAGCTGCTGAAG
PKS13_Check_Fw	TCTGCGGAAGTGATCTGCTCGCC
PKS13_Check_Rv	GGCTGCTTCCGCACACATCCG

B

Plasmids	Characteristics
pK18mobSacB	A plasmid for gene deletion in *C. glutamicum*, KanR
pVK7	Shuttle vector for *C. glutamicum* and *E. coli*, KanR

Transparent Methods

Materials

LB medium, FM4-64, PicoGreen, and SYTOX green were purchased from Life Technologies (Carlsbad, CA, USA). Mitomycin C (MMC) and penicillin G were purchased from Nacalai Tesque Co., Inc. (Kyoto, Japan). (+)-Biotin and phophatidylinositol were purchased from FUJIFILM Wako Pure Chemical Corporation (Osaka, Japan). L-α-phosphatidyl-DL-glycerol (distearoyl) was purchased from Tokyo Kasei Kogyo, Co, Ltd. (Tokyo, Japan). Cardiolipin from bovine heart was purchased from Olbracht Serdary Research Laboratories (Toronto, Canada). 1,2-Dipalmitoyl-*rac*-glycerol was purchased from Merck (Darmstadt, Germany). All other chemicals used were from commercial sources and of analytical grade. *Corynebacterium glutamicum* NBRC 12168 (ATCC 13032) was supplied by National Institute of Technology and Evaluation (Chiba, Japan).

Bacterial strains and plasmids

Strains used in this study are listed in Table S1. Primers and plasmids used in this study are listed in Table S2.

The NCgl1682 deletion strain of *C. glutamicum* was constructed as follows. The *NCgl1682* upstream and downstream regions were amplified by PCR using NCgl1682_FR1_Fw/NCgl1682_FR1_Rv and NCgl1682_FR2_Fw/NCgl1682_FR2_Rv primer sets, respectively. The PCR products were integrated with pK18mobSacB by In-Fusion (Clontech Laboratories Inc., CA, USA). The resulting plasmid was transformed into *C. glutamicum* as follows (van der Rest et al, 1999). *C. glutamicum* was cultured in LB medium supplemented with 2% glucose (w/v) at 30 ºC. After culturing overnight, *C. glutamicum* was inoculated (OD_{600} = 0.2) in 100 mL of Epo medium containing 1 g tryptone, 0.5 g yeast extract, 1 g NaCl, 400 mg isoniazide, 2.5 g glycine and 0.1 mL of Tween 40 per 1 L. *C. glutamicum* was then cultured for 24 h at 18 ºC. The shaking speed was 120 rpm. After cultivation, the cells were collected by centrifugation (4,000 × *g*, 10 min). The cells were washed five times with 10% glycerol (v/v). Finally, the cells were resuspended in 500 µL of 10% glycerol. In total, 100 µL of the solution was used for electroporation. Electroporation was performed under the following conditions: 25 µF, 600 kΩ, and 2.5 kV. In total, 1 mL of brain-heart infusion medium supplemented with 91 g L^{-1} sorbitol was immediately added to the solution. The resulting solution was incubated at 46 ºC for 6 min. After heat shock, the solution was incubated for 30 ºC for 1 h. Transformants and deletion mutant were selected with 25 µg/mL kanamycin and 10% (w/v) sucrose, respectively. For complementation of NCgl1682, *NCgl1682* and upstream region (150 bp) were amplified by PCR using NCgl1682_Ex_Fw/NCgl1682_Ex_Rv primer set, and integrated with pVK7 vector by In-Fusion. The resulting plasmid was transformed into *C. glutamicum* as described above. Transformants were selected with 25 µg mL^{-1} kanamycin.

Culture conditions

All bacteria were preincubated in LB medium. After preincubation at 30ºC for 24 h and washing cells, *C. glutamicum* was inoculated in 100 mL of minimum medium (MM-1) consisting 80 g glucose, 30 g $(NH_4)_2SO_4$, 5.7 g Na_2SO_4•$7H_2O$, 6 g KH_2PO_4, 2 g NaCl, 3.9 mg $FeCl_3$, 1.77 mg $ZnCl_2$, 0.44 mg $CuSO_4$•$5H_2O$, 5.56 mg $(NH_4)_6Mo_7O_{24}$•$4H_2O$, 0.4 g $MgSO_4$, 40 mg $FeSO_4$•$7H_2O$, 84 mg $CaCl_2$, 500 µg thiamine•HCl, 0.1 g EDTA, and 100 µg biotin per 1 L. pH was adjusted to 7.2 with KOH. *C. glutamicum* was then grown at 30ºC for 20-24 h (end of growth phase). As for Δ*pks13* mutant of *C. glutamicum*, the cells were grown at 30ºC for 72 h. The shaking speed was 150 rpm. For MV induction, each of MMC and penicillin was added to MM-1 medium to final concentrations of 100 ng mL^{-1} MMC and 0.4 U mL^{-1}, respectively, in early exponential phase. After preincubation in LB medium at 37ºC for 72 h and washing cells, *M. smegmatis* was inoculated into 100 mL of minimum medium (MM-2) consisting 0.7% (v/v) glycerol, 1 g KH_2PO_4, 2.5 g Na_2HPO_4, 0.5 g asparagine, 50 mg ferric ammonium citrate, 0.5 g $MgSO_4$•$7H_2O$, 0.5 mg $CaCl_2$, 0.1 mg $ZnSO_4$ and 200 µg biotin per 1 L. pH was adjusted to 7.0 with KOH. *M. smegmatis* was then grown at 37ºC for 9 days. The shaking speed was 90 rpm. For MV induction, each of MMC and penicillin was added to MM-2 medium to final concentrations of 100 ng mL^{-1} MMC and 0.4 U mL^{-1}, respectively, after 24 h incubation (early exponential phase). *R. equi* was preincubated in LB medium at 37ºC for 24 h and inoculated into 50 mL of fresh LB medium. *R. equi* was then grown at 37ºC for 16 h. The shaking speed was 190 rpm. For MV induction, each of MMC and penicillin was added to the minimum medium to final concentrations of 100 ng mL^{-1} MMC and 0.4 U mL^{-1}, respectively, in early exponential phase.

MV purification and quantification

MVs were isolated and quantified as follows. Culture supernatants were filtered with 0.45 µm pore size PVDF filter (Merck, Darmstadt, Germany). The supernatants were then ultracentrifuged for 1 h at 150,000 × *g*, 4ºC. Pellet was resuspended in 400 µL of 45% iodixanol (Optiprep, AXIS-SHIELD, Dundee, Scotland) in a buffer containing 20 mM HEPES-NaOH (pH 7.0) and 0.85% NaCl. This solution was placed at the base of a 4 mL tube, and then 400 µL of 40, 35, 30, 25, 20, 15 and 10% iodixanol solutions were layered on the top of the suspended solution to make density gradient in the tube. The tube was immediately ultracentrifuged for 3 h at 10,0000 × *g*, 4 ºC. After the ultracentrifugation, a fraction (400-500 µL) containing purified MVs, which appeared as a band in upper middle of the tube, were collected and then washed with 20 mM HEPES-NaOH (pH 7.0) and 0.85% NaCl. Pellet was resuspended in the same buffer, and this solution was used for further analyses. MVs were quantified using the fluorescent dye FM4-64.

Size distributions and particle numbers of MVs

Size distributions and particle numbers of MVs were analysed by Nanosight NS300 (Nanosight Ltd., Malvern, United Kingdom). After washing with 2 mL of H_2O, diluted MV solution was injected into the apparatus. Flow pass was equilibrated with 1.0 mL of the MV solution before analyses. Measurement was performed for three times, and size distributions and particle numbers were analysed based on these data.

Microscopy

Confocal laser scanning microscopy (CLSM) was performed with LSM780 with Airyscan detector (Carl Zeiss, Oberkochen, Germany). For CLSM, bacteria were put on 0.8% agarose pad after staining with 2.5 μg mL^{-1} FM4-64 or 3 μM acridine orange 10-nonyl bromide. Peptidoglycan was stained by culturing bacteria in MM-1 medium containing 10 μM HADA followed by washing cells with fresh MM-1 medium. For live-cell imaging, bacteria were put on MM-1 containing 0.8% agarose, 2.5 μg mL^{-1} FM4-64, 5 μM SYTOX green and 0.1 or 100 μg L^{-1} biotin after staining cells with 2.5 μg mL^{-1} FM4-64. In total, 400 ng mL^{-1} MMC or 0.4 U mL^{-1} was added to the above medium when required. The cells were then incubated and observed at 30ºC.

For transmission electron microscopy (TEM), purified MVs were attached to thin carbon film-coated TEM grids (ALLIANCE Biosystems, Osaka, Japan) and washed with H_2O. MVs were then visualised by negative staining. For TEM inspection of ultra-thin sections of bacterial cells, cells were fixed with a solution containing 100 mM phosphate buffer (pH 7.0) and 2% glutaraldehyde. After the first fixation, the cells were washed twice with 0.1 M phosphate buffer and then further fixed with 2% OsO_4. After the second fixation, the cells were dehydrated with 50%, 70% and 100% ethanol sequentially. The cell suspension was replaced with propylene oxide solution and then embedded in Epon 812. The samples were sliced by ultramicrotome and the resulting ultra-thin sections were visualised with uranyl acetate and lead-containing staining solution.

Quick-freeze, deep-etch electron microscopy

Samples were treated as previously reported (Tulum et al, 2019). MVs were collected by centrifugation at 150,000 × *g*, at 4 ºC for 60 min and suspended in water. The sample suspension was mixed with a slurry that included mica flakes, placed on a rabbit lung slab, and frozen by a metal contact method with CryoPress (Valiant Instruments, St. Louis, MO, USA) cooled by liquid helium. The slurry was used to retain an appropriate amount of water before freezing unless stated in the figure legend. 80% glycerol instead of water when observing the inner leaflet of the lipid bilayer. The specimens were fractured and etched for 15 min at −104°C, in a JFDV freeze-etching device (JEOL Ltd., Akishima,Japan). The exposed MVs were rotary-shadowed by platinum at an angle of 20 degrees to be 2 nm in thickness and backed with carbon. Replicas were floated off on full-strength hydrofluoric acid, rinsed in water, cleaned with a commercial bleach, rinsed in water and picked up onto copper grids as

described. Replica specimens were observed by a JEM 1010 transmission electron microscope (JEOL, Tokyo, Japan) at 80 kV equipped with a FastScan-F214 (T) CCD camera (TVIPS, Gauting, Germany).

Quantification of extracellular double-stranded DNA

Bacteria were grown as described in Culture conditions and removed by centrifugation (7,000 *g* × 10 min). Double-stranded DNA in the resulting supernatant was then quantified using PicoGreen (Life Technologies, Carlsbad, CA, USA). DNA concentration was calculated based on the standard curve obtained from the standard DNA.

Chromatography and mass spectrometry

Liquid chromatography/mass spectrometry (LC/MS) analyses were carried out using Nexera X2 system and an LCMS-8050 (Shimadzu, Kyoto, Japan) equipped with a Kinetex EVO C18 2.6 µm 150 mm × 2.1 mm (PHENOMENEX, Torrance, CA, USA), ZIC-HILIC 3.5 µm 150 mm × 2.1 mm (Merck, Darmstadt, Germany) or TSK-gel ODS-120H 3 µm 2.0 × 150 mm (Tosoh Co., Ltd., Tokyo, Japan). Lipids were analysed using the following conditions: Kinetex EVO C18 column; flow rate, 0.26 mL min^{-1}; temperature, 40ºC; solvent A, H_2O:acetonitrile = 40:60 (v/v) and 10 mM ammonium formate; and solvent B, acetonitrile:2-propanol = 10:90 (v/v) and 10 mM ammonium formate. After column equilibration with 100% solvent A, 2 µl of a sample was injected into the column. The samples were eluted from the column by the following gradient: 0-20 min, 0-100% solvent B; 20-30 min, 100% solvent B; 30-35 min, 0% solvent B. Mycolic acid esters were detected by LC/MS/MS as follows. Mycolic acid esters were detected as $[M+NH_4]^+$ adduct in the positive ion mode and their structures were confirmed by MS/MS analysis with a collision energy -30 or -40 eV.

Amino acids were analysed using the following conditions: ZIC-HILIC column; flow rate, 0.2 mL min^{-1}; temperature, 40ºC; solvent A, H_2O:acetonitrile:formate = 98:1:1 (v/v); and solvent B, H_2O:acetonitrile:formate = 1:98:1 (v/v). After column equilibration with 95% solvent B, 2 µl of a sample was injected into the column. The samples were eluted from the column by the following gradient: 0-1 min, 95% solvent B; 1-10 min, 95-5% solvent B; 10-14 min, 5% solvent B; 14-21 min, 95% solvent B. Concentrations of the samples were calculated based on the standard curve obtained from the standard solution. Amino acids were detected by multiple reaction monitoring (MRM) mode as follows. Alanine (*m/z* = 89.9 $[M+H]^+$), glutamate (*m/z* = 148.2 $[M+H]^+$) and *meso*-diaminopimelic acid (*m/z* = 191.0 $[M+H]^+$) were fragmented into product ions which exhibit *m/z* values of 44.1, 84.2 and 128.1, respectively, and detected. Collision energies were -13.0 eV, -18.0 eV and -15.0 eV, respectively.

Sugars were analysed using the following conditions: TSK-gel ODS column; flow rate, 0.2 mL min^{-1}; temperature, 40ºC; solvent A, H_2O:acetonitrile:formate = 98:1:1 (v/v) and 5 mM ammonium acetate; and solvent B, H_2O:acetonitrile:formate = 1:98:1 (v/v). After column equilibration with 100% solvent A, 2 µl of a sample was injected into the column. The samples were eluted from the column by the

following gradient: 0-20 min, 0-100% solvent B; 20-25 min, 0% solvent B. Sugars were derivatized (described below) and detected by MRM mode as follows. Arabinose (*m/z* = 481.1 $[M+H]^+$), *N*-acetylglucosamine (*m/z* = 510.1 $[M+H]^+$) and galactose (*m/z* = 511.3 $[M+H]^+$) were fragmented into a product ion which exhibits *m/z* value of 175.2 and detected. Collision energies were -30.0 eV, -32.0 eV and -29.0 eV, respectively.

Gas chromatography/mass spectrometry (GC/MS) analyses were carried out using GC2010 and GCMS-QP2010 (Shimadzu, Japan) equipped with FFAP silica capillary column 0.25 mm × 25 m × 0.25 μm (QUADREX Corp., Woodbridge, CT, USA). Fatty acids including mycolic acids were separated and detected under the following conditions: injector temperature, 320ºC; the flow rate of carrier gas (helium), 24 mL min^{-1}. The sample were eluted from the column by the following temperature gradient: 0-2 min, 80ºC; 2-9 min, 80-220ºC; 9-34 min, 320ºC.

Extracted lipids were separated by thin layer chromatography (TLC) as follows. Samples were spotted onto a silica gel plate and then separated using chloroform:methanol:H_2O = 65:25:4 (v/v, for corynomycolic acid esters and polar lipids), chloroform: hexane: methanol: acetate = 50:30:10:5 (v/v, for phosphatidylglycerols and cardiolipins) and toluene: chloroform: acetone = 7:2:1 (v/v, for diacylglycerols) as the solvents. Based on a previous study (Bansal-Mutalik et al, 2011), L-α-phosphatidyl-DL-glycerol (distearoyl), phophatidylinositol, cardiolipin from bovine heart and 1,2-dipalmitoyl-*rac*-glycerol were used as standards. Silica gel plate was then dried and sprayed with 0.01% (w/v) primuline (in 80% acetone). Fluorescence of the labelled lipids were detected with UV at 365 nm. Obtained images were analysed by ImageJ (Schneider et al, 2012). Amounts of lipids were calculated based on the standard curve of intensities of the above lipid standards.
Matrix-assisted laser desorption/mass spectrometry (MALDI-TOF/MS) was performed using UltrafleXtreme-ETA MALDI-TOF/TOF (Bruker, Billerica, MA, USA). 2-Cyano-3-(4-hydroxyphenyl) acrylic acid was used as a matrix.

Analyses of glutamate and lysine effluxes

Glutamate and lysine were detected and quantified as follows. After culturing *C. glutamicum*, the cells were removed by centrifugation (7,000 *g* × 10 min). Equivalent volume of acetonitrile was added to the resulting supernatant. This solution was filtered (0.45 μm) and then analysed by LC/MS. Cells were lyophilised and then suspended in 50% acetonitrile. After removing debris by centrifugation (20,000 *g* × 5 mi), the resulting supernatant was analysed by LC/MS. The extracted amino acids were separated as described under the above section Chromatography and mass spectrometry, and then detected by MRM mode. Detection conditions for glutamate were as follows: retention time, 8.6 min; a precursor ion, *m/z* = 148.2; a product ion, *m/z* = 84.2; collision energy, -16.0 eV; detection mode, positive. Detection conditions for lysine were as follows: retention time, 10.6 min; a precursor ion, *m/z* = 147.1; a product ion, *m/z* = 84.2; collision energy, -17.0 eV; detection mode, positive. Amounts of

glutamate and lysine were calculated based on the standard curve of the intensities obtained from authentic standards. 1.6 μL mg^{-1} dry cell weight (Nakamura et al, 2007) was used to calculate intracellular glutamate concentrations.

Analyses of lipids and sugars

For GC/MS analyses, lipids were extracted and derivatised as follows. Lyophilised cells (80 mg) and MVs (6~17 mg) were suspended in 500 μL of 10% KOH (in methanol). This solution was incubated at 98ºC for 2 h. After acidification (< pH 2) by adding 6 N HCl, lipids were then extracted by hexane. After removing the solvent, lipids were further incubated and esterified in benzene: methanol: sulfate: = 10:20:1 (v/v) at 98ºC for 2 h. H_2O was then added to the solution, and lipids were extracted by hexane. Covalently bound-mycolic acids of mycolic acid-arabinogalactan-peptidoglycan complexes were extracted and derivatised as described above using purified cell walls (see below). After removing the solvent, 50 μL of pyridine and 100 μL of *N,O*-bis(trimethylsilyl)trifluoroacetamide (BSTFA) were added to the lipids. After incubation at 70ºC for 12 h, the derivatised lipids were subjected to GC/MS analyses.

For LC/MS analyses, lipids are extracted as follows. After cultivation for 12~16 h (the end of exponential phase), cultured cells were harvested by centrifugation and washed with 0.85% NaCl. Cells were then suspended in H_2O-saturated 1-butanol. 1-Butanol extraction was previously reported to potentially enrich mycomembrane lipids of mycolic acid-containing bacteria (Klatt et al, 2018; Morita et al, 2005; Patterson et al, 2000). The cells were removed by centrifugation and resuspended in chloroform: methanol = 2:1. The same extraction was then performed using chloroform: methanol: H_2O = 1:2:0.8. Lipids of MV fractions were extracted by chloroform: methanol = 2:1. All extracts were dried, dissolved with the corresponding solvent, and then subjected to LC/MS analyses. In these analyses, we defined the mycomembrane-specific lipids and the inner membrane-specific lipids as the lipids that were detected in either the mycomembrane (1-butanol extract) or the inner membrane extract (total of chloroform/methanol and chloroform/methanol/water extracts).

Membrane lipids in *C. glutamicum* were identified as follows. Based on our results of GC/MS analyses of derivatised fatty acids (Fig. S12), C16-C18 fatty acids and mycolic acids (C32 and C34) were identified to be major acyl chains consisting mycomembrane and inner membrane lipids of *C. gltamicum* under the tested condition. In addition, previous studies (Bansal-Mutalik et al, 2011; Klatt et al, 2018) and our TLC analysis (Fig. 3 and Fig. S15) showed that trehalose dicorynomycolic acids, phosphatidylglycerol, diacylglycerol, phosphatidylinnositols (including the mannoside derivatives) and cardiolipins are major classes of lipids consisting the membranes. Considering these observations, on LC/MS, we scanned the major membrane lipids in each of the extracts using the theoretical *m/z* values that were calculated from the possible structures of the lipids containing C32-C34 corynomycolic acids or C16-C18 fatty acids

(Hoischen et al, 1990; Klatt et al, 2018). From the result of this analysis, candidate molecules that might belong to each class of lipids were listed. The structures of the candidate lipids were then determined by LC/MS/MS analysis based on *m/z* values of the fragments including the fatty acid moieties and the polar head group moieties. Profiles of the identified lipids of *C. glutamicum* was consistent with those in the previous studies (Cox et al, 2009; Hsu et al, 2001, 2007; Kind et al, 2013; Minkler et al, 2010; Mishra et al, 2009). The characteristics of the fragment patterns of the identified lipids are summarised in Fig. S16. Representative data of LC/MS/MS analysis and the catalogue of the identified lipids are shown in Fig. S16 and S17. Ion intensities of the detected lipids in the scanning mode on LC/MS are shown in Fig. S18.

Cell walls were purified from cells and MVs as follows. *C. glutamicum* cells were disrupted by sonication and centrifuged (5,000 *g* × 30 min and 20,000 *g* × 30 min). 4% (w/v) sodium dodecyl sulfate was added to the pellets and the resulting solutions were incubated at 100ºC for 40 min. 10% tween 40 was added to the purified MVs and the resulting solutions were incubated at room temperature for 40 min. After incubation, these solutions were centrifuged (20,000 *g* × 30 min at 20ºC) and washed with H_2O. The resulting pellets were lyophilised and stored at -20ºC. For LC/MS analyses, the lyophilised cell walls were hydrolysed by 6 N HCl at 100ºC for 3 h. These solutions were then dried and subjected to LC/MS analyses for amino acids or further derivatisation. Dried cell wall components were dissolved with 10 µL of H_2O. 15 µL of 0.5 M NaOH and 25 µL of 0.5 M 3-methyl-1-phenyl-5-pyrazolone (PMP) were then added to the solutions. After incubation at 70ºC for 2 h, 20 µL of 0.5 N HCl was added to these solutions. The resulting solutions were subjected to LC/MS analyses for PMP-derivatised sugars. Amino acids and sugar derivatives were detected by MRM mode. The amounts of amino acids and sugars were quantified based on the standard curve obtained from intensities of authentic standards.

Identification of proteins

Proteins were identified as follows. Cells were disrupted by sonication and the lysates were used for further experiment. The cell lysate and purified MVs solutions were mixed with an equivalent volume of a sample buffer containing 0.1 M Tris-HCl (pH 6.8), 20% (v/v) glycerol, 4% (w/v) SDS, 5% (v/v) 2-mercaptoethanol and 0.2% (w/v) bromophenol blue, and incubated at 98ºC for 5 min. After incubation, these solutions were applied to a gel and then subjected to an electrophoresis. Stacking gel contained 0.15 mL of 30% (w/v) acrylamide/bis mixed solutions (Nacalai Tesque Co., Inc., Kyoto, Japan), 0.25 mL of 1.5 M Tris-HCl (pH 8.8), 10 µL of 10% (w/v) ammonium persulfate and 2 µL of tetramethylethylenediamine per 1 mL. Running gel contained 1.6 mL of 30% acrylamide/bis mixed solutions, 1 mL of 1.5 M Tris-HCl (pH 8.8), 20 µL of 10% (w/v) ammonium persulfate and 4 µL of tetramethylethylenediamine per 4 mL. After the electrophoresis, bands derived from the proteins were stained with Coomassie brilliant blue and then cut out from the gel. Isolated proteins were degraded by trypsin, and then carbamidomethyl group was added to -SH group of cysteine residues of the peptides. The resulting peptides were analysed by MALDI-TOF/MS. Obtained mass spectra derived from these

peptides were analysed by MASCOT database search (Matrix Science Ltd., London, United Kingdom). Proteins that were derived from *C. glutamicum* ATCC13032 and showed the highest MASCOT scores (above significance threshold) were assigned to the bands.

Supplemental References

Armenteros, J. J. A., Tsirigos, K. D., Sønderby, C. K., Petersen, T., N., Winther, O., Brunak, S., von Heijne, G., and Nielsen, H. (2019). SignalP 5.0 improves signal peptide predictions using deep neural networks. Nat. Biotechnol. *37*, 420-423.

Bansal-Mutalik, R., and Nikaido, H. (2011). Quantitative lipid composition of cell envelopes of *Corynebacterium glutamicum* elucidated through reverse micelle extraction. Proc. Natl. Acad. Sci. USA *108*, 15360-15365.

Brennan, P. J., and Nikaido, H. (1995). The envelope of mycobacteria. Annual Reviews of Biochemistry *64,* 29-63.

Bukovski, A. (2013). Cell envelope of Corynebacteria: structure and influence on pathogenicity. ISRN Microbiol. 2013:935736.

Cox, D., Fox, L., Tian, R., Bardet, W., Skaley, M., Mojsilovic, D., Gumperz, J., and Hildebrand, W. (2009). Determination of cellular lipids bound to human CD1d molecules. PLoS One 4:e5325.

Hashimoto, K., Kawasaki, H., Akazawa, K., Nakamura, J., Asakura, Y., Kudo, T., Sakuradani, E., Shimizu, S., and Nakamatsu, T. (2006). Changes in composition and content of mycolic acids in glutamate-overproducing *Corynebacterium glutamicum*. Biosci. Biotechnol. Biochem. *70*, 22-30.

Hoischen, C., and Kräman, R. (1990). Membrane alteration in necessary but not sufficient for effective glutamate secretion in *Corynebacterium glutamicum*. J. Bacteriol. *172*, 3409-3416.

Hsu, F. F., Turk, J., Owens, E. R., and Russell, D. G. (2007). Structural characterization of phosphatidyl-*myo*-inositol mannosides from *Mycobacterium bovis* Bacillus Calmette Guérin by multiple-stage quadrupole ion-trap mass spectrometry with electrospray ionization. I. PIMs and lyso-PIMs. J. Am. Soc. Mass Spectrom. *18*, 466-478.

Hsu, F. F., and Turk, J. (2001). Studies on phosphatidylglycerol with triple quadrupole tandem mass spectrometry with electrospray ionization: fragmentation processes and structural characterization. J. Am. Soc. Mass Spectrom. *12*, 1036-1043.

Kind, T., Liu, K. H., Lee, D. Y., DeFelice, B., Meissen, J. K., and Fiehn, O. (2013). LipidBlast *in silico* tandem mass spectrometry database for lipid identification. Nature Methods *10*, 755-758.

Klatt, S., Brammananth, R., O'Callaghan, S., Kouremenos, K. A., Tull, D., Crellin, P. K., Coppel, R. L., and McConville, M. J. (2018). Identification of novel lipid modifications and intermembrane dynamics in *Corynebacterium glutamicum* using high-resolution mass spectrometry. J. Lipid Res. *59*, 1190-1204.

Minkler, P. E., and Hoppel, C. L. (2010). Separation and characterization of cardiolipin molecular species by reverse-phase ion pair high-performance liquid chromatography-mass spectrometry. J. Lipid Res. *51*, 856-865.

Mishra, A. K., Batt, S., Krumbach, K., Eggeling, L., and Besra, G. S. (2009). Characterization of the *Corynebacterium glutamicum* Δ*pimB'* Δ*mgtA* double deletion mutant and the role of *Mycobacterium tuberculosis* orthologues Rv2188c and Rv0557 in glycolipid biosynthesis. J. Bacteriol. *191*, 4465-4472.

Mitaku, S., Hirokawa, T., and Tsuji, T. (2002). Amphiphilicity index of polar amino acids as an aid in the characterization of amino acid preference at membrane-water interfaces. Bioinformatics *18*, 608-616.

Morita, Y. S., Velasquez, R., Taig, E., Waller, R. F., Patterson, J. H., Tull, D., Williams, S. J., Billman-Jacobe, H., and McConville, M. J. (2005). Compartmentalization of lipid biosynthesis in Mycobacteria. J. Biol. Chem. *280*, 21645-21652.

Nakamura, J., Hirano, S., Ito, H., and Wachi, M. (2007). Mutations of the *Corynebacterium glutamicum* NCgl1221 gene, encoding a mechanosensitive channel homolog, induce L-glutamic acid production. Appl. Environ. Microbiol. *73*, 4491-4498.

Patterson, J. H., McConville, M. J., Haites, R. E., Coppel, R. L., and Billman-Jacobe, H. (2000). Identification of a methyltransferase from *Mycobacterium smegmatis* involved in glycopeptidolipid synthesis. J. Biol. Chem. *275*, 24900-24906.

Portevin, D., Sousa-D'Auria, C. D., Houssin, C., Grimaldi, C., Chami, M., Daffé, M., and Guilhot, C. (2004). A polyketide synthase catalyzes the last condensation step of mycolic acid biosynthesis in mycobacteria and related organisms. Proc. Natl. Acad. Sci. USA *101*, 314-319.

Schneider, C.A., Rasband, W.S., and Eliceiri, K.W. (2012). NIH Image to ImageJ: 25 years of image analysis. Nat. Methods *9*, 671-675.

Tulum I., Tahara, Y. O., and Miyata, M. (2019). Peptidoglycan layer and disruption processes in *Bacillus subtilis* cells visualized using quick-freeze, deep-etch electron microscopy. Microscopy *68*, 441-449.

van der Rest, M. E., Lange, C., and Molenaar, D. (1999). A heat shock following electroporation induces highly efficient transformation of *Corynebacterium glutamicum* with xenogeneic plasmid DNA. Appl. Microbiol. Biotechnol. *52*, 541-545.